Endophilin A1 facilitates organization of the GABAergic postsynaptic machinery to maintain excitation-inhibition balance

Xue Chen[1,2], Deng Pan[1,2], Jia-Jia Liu[1,2*] and Yanrui Yang[1*]

[1]State Key Laboratory of Molecular Developmental Biology, Institute of Genetics and Developmental Biology, Chinese Academy of Sciences, Beijing 100101, China

[2]College of Life Sciences, University of Chinese Academy of Sciences, Beijing 100039, China

*Correspondence to Yanrui Yang: yryang@genetics.ac.cn; Jia-Jia Liu: jjliu@genetics.ac.cn.

Abstract

The assembly and operation of neural circuits in the brain rely on the coordination and balance of excitatory and inhibitory activities. Inhibitory synapses are key regulators of the functional balance of neural circuits. However, due to the diversity of inhibitory presynaptic neurons, the complex composition of postsynaptic receptor subunits and the lack of typical postsynaptic dense structure, there are relatively few studies on the regulatory mechanisms for inhibitory synaptic structure and function, and insufficient understanding of the cellular and molecular abnormalities of inhibitory synapses in neurological and neuropsychiatric disorders. Here, we report a crucial role for endophilin A1 in inhibitory synapses. We show that endophilin A1 directly interacts with the inhibitory postsynaptic scaffold protein gephyrin in excitatory neurons, and promotes organization of the inhibitory postsynaptic density and synaptic recruitment/stabilization of the γ-aminobutyric acid type A receptors via its plasma membrane association and actin polymerization promoting activities. Loss of endophilin A1 by gene knockout in mouse hippocampal CA1 pyramidal cells weakens inhibitory synaptic transmission and causes imbalance in the excitatory/inhibitory function of neural circuits, leading to increased susceptibility to epilepsy. Our findings identify endophilin A1 as an iPSD component and provide new insights into the organization and stabilization of inhibitory postsynapses to maintain E/I balance as

well as the pathogenesis of epilepsy.

Key words: endophilin A1, E/I balance, epilepsy, $GABA_AR$, gephyrin, inhibitory synapse

Introduction

The excitatory and inhibitory synaptic activities of neural circuits are tightly orchestrated in the central nervous system (Sakimoto et al., 2021). The imbalance between excitatory and inhibitory neuronal activity is implicated in many neurological and neuropsychiatric diseases including schizophrenia, autism spectrum disorder and epilepsy (Canitano and Pallagrosi, 2017; Canitano and Palumbi, 2021; Foss-Feig et al., 2017; Fritschy, 2008). In the brain, in contrast to asymmetric excitatory synapses formed between axonal boutons and dendritic postsynaptic structures with thick disc-shaped PSD, inhibitory synapses are symmetric and are constituted of the presynaptic terminal from diverse interneurons and the postsynaptic plasma membrane with thin sheet-like PSD where receptor complexes are anchored (Bai et al., 2021; Favuzzi et al., 2019; Liu et al., 2020; Mody and Pearce, 2004; Tao et al., 2018). Although the formation, maturation and plasticity of both excitatory and inhibitory synapses are vitally important for neural circuit functioning, much more research efforts have been focused on the regulatory mechanisms governing excitatory synaptic structure and function. The mechanisms by which inhibitory synapses are constructed in the brain and fine-tuned in response to neural activity remain largely unexplored.

The γ-aminobutyric acid type A receptors ($GABA_ARs$), major targets of antiseizure drugs, are heteropentameric chloride channels that mediate fast synaptic transmission at inhibitory synapses in the brain (Scott and Aricescu, 2019). Several neuropathologies are characterized by alterations in $GABA_A$ receptor trafficking, synaptic E/I ratio and neuronal excitability (Sakimoto et al., 2021). At the inhibitory postsynaptic site, synaptic localization and functioning of $GABA_ARs$ requires trans-synaptic cell adhesion molecules, submembranous scaffold proteins and

intracellular signaling proteins. Gephyrin is a master organizer of iPSD, which self-assembles into planar lattices beneath the plasma membrane and anchors $GABA_A$Rs or glycine receptors (GlyRs) to the postsynaptic sites (George et al., 2021; Kasaragod and Schindelin, 2019; Kirsch et al., 1991; Tyagarajan and Fritschy, 2014). Collybistin, a membrane lipid-binding protein, functions in recruitment of gephyrin and $GABA_A$Rs to the plasma membrane by interacting with gephyrin, the synaptic adhesion molecule neuroligin-2 (NL-2) and the α2 subunit of $GABA_A$Rs (Kalscheuer et al., 2009; Kins et al., 2000; Poulopoulos et al., 2009; Saiepour et al., 2010). The transmembrane protein Shisa7 binds $GABA_A$Rs and regulates their trafficking, synaptic abundance and functional properties via binding to protein(s) other than gephyrin (Han et al., 2019; Liu et al., 2020). Nevertheless, mechanisms governing the assembly, recruitment and maintenance of various inhibitory synaptic components remain largely enigmatic.

The majority of inhibitory synapses are formed on the dendritic shaft, or around the cell body of excitatory principal neurons where both actin and microtubule cytoskeletons are present underneath the plasma membrane. Through direct interaction with polymerized tubulin, gephyrin organizes the iPSD by anchoring the GlyRs and $GABA_A$Rs to the microtubule cytoskeleton (Parato and Bartolini, 2021). Notably, although small F-actin patches are observed within the dendritic shaft where the majority of inhibitory synapses are assembled (van Bommel et al., 2019), role(s) of the actin cytoskeleton in the organization and maintenance of inhibitory synapses is still unclear.

Endophilin A1 (EEN1) is a member of the endophilin A protein family characterized by an amino (N)-terminal membrane-binding N-BIN/amphiphysin/Rvs (BAR) domain and a carboxyl (C)-terminal Src homology 3 (SH3) domain. The gene encoding endophilin A1 (*EEN1*, gene name *sh3gl2*) is almost exclusively expressed in the brain (Ringstad et al., 1997), and has been implicated in epilepsy, schizophrenia, depression, Parkinson's disease, and Alzheimer's disease (Chang et al., 2017; Corponi et al., 2019; Germer et al., 2019; Ren et al., 2008; Yu et al., 2018a; Yu et al., 2018b).

In excitatory synapses, endophilin A1 functions in synaptic vesicle recycling and autophagosome formation at the axon terminal (Bademosi et al., 2023; Milosevic et al., 2011; Murdoch et al., 2016; Ringstad et al., 1999; Schuske et al., 2003; Soukup et al., 2016; Verstreken et al., 2003; Watanabe et al., 2018), and regulates the morphogenesis, maturation, and acute structural plasticity of dendritic spines by promoting actin polymerization via its effector protein p140Cap (Yang et al., 2021; Yang et al., 2018; Yang et al., 2015).

Previous studies reported that the double knockout (KO) mice of *EEN1* and *EEN2* exhibit spontaneous epileptic seizures (Milosevic et al., 2011). However, *EEN1* depletion only causes a slight decrease in excitatory synaptic transmission in hippocampal CA1 neurons (Yang et al., 2021; Yang et al., 2018). As E/I imbalance is caused by changes in either excitatory or inhibitory activity, or both, we were prompted to investigate the biological function of endophilin A1 in the inhibitory synapses. In this study, we show that endophilin A1 interacts with gephyrin and localizes to GABAergic postsynapses. Via its membrane-binding and actin polymerization-promoting activities, endophilin A1 facilitates organization of the inhibitory postsynaptic machinery. Loss of endophilin A1 causes impairment of inhibitory synaptic transmission, E/I imbalance and aggravation of epileptic susceptibility.

Results

Ablation of endophilin A1 causes E/I imbalance and increases epilepsy susceptibility

Previous studies found that *EEN1* and *EEN2* double knockout (KO) mice exhibit spontaneous epileptic seizures (Milosevic et al., 2011), suggesting that endophilin A1 and A2 are involved in maintaining the E/I balance. However, another study reported that the protein levels of endophilin A1 were higher in temporal neocortex neurons of temporal lobe epilepsy (TLE) patients (Yu et al., 2018b). Moreover, in a chemical kindling mouse model of epilepsy, in which mice are chronically induced with the

GABA$_A$R antagonist pentylenetetrazole (PTZ) (Dhir, 2012), endophilin A1 was also upregulated in the hippocampus and adjacent temporal cortex , and silencing its expression in the hippocampal CA3 region reduced PTZ-induced seizure susceptibility and severity (Yu et al., 2018b). To investigate the role of endophilin A1 in epilepsy, we determined the impact of *EEN1* gene ablation on chemical kindling of pan-neural *EEN1* KO mice (Yang et al., 2018) with PTZ at a sub-convulsive dose of 25 mg/kg. Compared with the wild-type, PTZ-induced epileptic behaviors were significantly exacerbated in *EEN1* KO mice (Figure 1A-C and Video S1).

We previously found that *EEN1* KO caused a slight decrease in the amplitude of evoked excitatory postsynaptic currents (eEPSC) and a significant attenuation of long-term potentiation (Yang et al., 2018). As imbalance between excitatory and inhibitory signals in neuronal circuits is implicated in epilepsy, we then determined whether loss of endophilin A1 in excitatory neurons affects the E/I ratio by electrophysiological analysis. To this end, we eliminated the *EEN1* gene in pyramidal neurons by stereotaxic injection of adeno-associated virus (AAV) expressing CaMKIIα promoter-driven Cre recombinase into the hippocampal CA1 region of *EEN1*$^{fl/fl}$ mice (Figure 1D). Whole-cell patch clamp recording of CA1 pyramidal cells indicated that, while the eEPSC and its paired-pulse ratio were not significantly changed, the evoked inhibitory postsynaptic current (eIPSC), not its PPR, was decreased in the *EEN1* KO neurons, resulting in a significant increase in the E/I ratio (Figure 1E-I). Of note, neither the frequency nor the amplitude of miniature EPSCs (mEPSC) or miniature IPSCs (mIPSC) was altered in *EEN1* KO neurons (Figure 1J-O). Moreover, neither fast mIPSCs (perisomatic events: < 2.8 ms) nor slow mIPSCs (distal dendritic events: > 2.8 ms) (Miles et al., 1996) were affected by *EEN1* KO (Figure S1), indicating that presynaptic quantal release of soma- or dendrite-targeting inhibitory synapses is normal. Taken together, these data indicate that endophilin A1 in hippocampal pyramidal neurons functions in inhibitory synaptic transmission to maintain E/I balance.

Endophilin A1 is required for the formation and stabilization of inhibitory synapses

Diminished eIPSC in *EEN1*$^{-/-}$ pyramidal neurons prompted us to determine the role of endophilin A1 in inhibitory synapses by immunofluorescence staining of brain sections from *EEN1*$^{-/-}$ mice. Analysis of confocal microscopy images revealed that, compared with the wild-type, there was a significant decrease in fluorescent signals of both VGAT and gephyrin, the inhibitory pre- and post-synaptic markers, and PSD95, the excitatory postsynaptic marker, in all subregions of the hippocampus of the *EEN1*$^{-/-}$ mice on postnatal day 21 (P21) (Figure 2A,C,D,F, and S2A,S2C), suggesting defects in synapse development. The decreases in inhibitory but not excitatory postsynaptic protein were also detected in the *EEN1*$^{-/-}$ mice at P60 (Figure 2B,C,E,F, and S2B,S2C), indicating that the assembly and/or stabilization of inhibitory postsynapses was impaired throughout brain development. Notably, gephyrin signals in all layers of the hippocampal subregions were reduced in the *EEN1*$^{-/-}$ mice (Figure S2D and S2E). As different types of interneurons synapse with hippocampal excitatory neurons at distinct subcellular compartments (soma, axon initial segment, proximal and distal dendrites) indicated by the layered structures of the hippocampus (Spruston, 2008), these data suggest that endophilin A1 functions in the assembly/stabilization of inhibitory synapses formed between various presynaptic neurons and postsynaptic neurons.

Next we analyzed the $GABA_A$ receptors and found that, consistent with changes in inhibitory postsynaptic marker, signals of the $GABA_AR$ γ2 subunit were decreased in the hippocampi of both juvenile and adult *EEN1*$^{-/-}$ mice (Figure 2G-I). These data collectively indicate that endophilin A1 orchestrates the assembly of inhibitory synapses, the architecture of inhibitory postsynapses in particular, and functioning of GABAergic synapses.

Endophilin A1 localizes to the iPSD and augments the organization of the inhibitory postsynaptic machinery

To substantiate the role of postsynaptic endophilin A1 in the assembly of inhibitory synapses and exclude the impacts of presynaptic endophilin A1 and its depletion on early embryonic development, we determined the effects of endophilin A1KO on inhibitory and excitatory synapses in cultured hippocampal pyramidal neurons during late developmental stages. As the expression levels of $GABA_AR$ α1 are highly heterogeneous in individual cultured neurons (Figure S3), we determined the effect of Cre-mediated *EEN1* KO on surface expression of $GABA_AR$ γ2 in *EEN1*$^{fl/fl}$ hippocampal neurons by immunofluorescence staining. Whilst no changes in surface GluA1 was detected, the fluorescence signal intensity and number of surface $GABA_AR$ γ2 clusters were largely lower in dendrites of *EEN1* KO neurons, which was rescued by re-expression of endophilin A1 (Figure 3A-D). We further examined the total and surface levels of synaptic proteins by immunoblotting. Biotinylation assay of surface proteins revealed that, compared with wild-type, although there was no change in total levels of synaptic proteins in *EEN1* KO pyramidal neurons, the surface expression of $GABA_ARs$ but not NL2 or the NR1 subunit of the NMDA-type glutamate receptor was significantly reduced (Figure 3E,F). Collectively, these data indicate that postsynaptic endophilin A1 enhances the surface clustering of $GABA_ARs$ and facilitates the assembly of inhibitory postsynapses in pyramidal neurons.

Next we sought to determine the molecular function of endophilin A1 in inhibitory synapses at the cellular level. By immunofluorescence staining and super-resolution microscopy of hippocampal neurons in dissociated culture, we observed partial colocalization of endophilin A1 with gephyrin as well as surface $GABA_AR$ γ2 in dendrites of hippocampal neurons, and juxtaposition or partial colocalization of endophilin A1 and VGAT puncta (Figure 3G-I and Video S2-4), indicating that endophilin A1 localizes to not only ePSD but also iPSD. Therefore, we speculated that endophilin A1 acted as a component of iPSD. Previous studies reported that synaptic $GABA_ARs$ contain the γ2 subunit along with α and β subunits (e.g., α1β2γ2) (Scott and Aricescu, 2019). The γ2 subunit is essential for receptor clustering at the synapse, mediated by interactions with scaffold proteins (Essrich et

al., 1998). Indeed, co-immunoprecipitation (coIP) of endogenous proteins in membrane fractions from mouse brain lysates with antibodies against $GABA_AR$ α1 detected not only the known iPSD components γ2, NL2 and gephyrin, but also endophilin A1, and vice versa (Figure 3J). Of note, loss of endophilin A1 caused decreases in levels of $GABA_AR$ γ2 and gephyrin but not NL2 in anti-$GABA_AR$ α1 immunoprecipitates (Figure 3K). Further, immunoblotting of synaptosome fractions revealed that the levels of $GABA_AR$ γ2 and gephyrin were reduced at synapses in adult *EEN1* KO mice (Figure 3L). Together, these data support that endophilin A1 functions at the iPSD to promote the assembly and/or stabilization of the GABAergic postsynaptic machinery.

Endophilin A1 directly interacts with the scaffold protein gephyrin and promotes its clustering and localization of $GABA_ARs$ to iPSD

We subsequently sought to investigate the mechanistic role of endophilin A1 in the clustering of inhibitory postsynaptic proteins. To this end, we performed coIP from mouse brain lysates with antibodies against endophilin A1 (Figure 4A) and analyzed the immunoprecipitates by mass spectrometry. Gene Ontology (GO) analysis revealed that, in addition to proteins participating in known cellular processes involving endophilin A1, such as synaptic vesicle recycling, actin cytoskeleton remodeling, endocytosis and long-term potentiation (Gad et al., 2000; Ringstad et al., 1999; Schuske et al., 2003; Verstreken et al., 2003; Yang et al., 2021; Yang et al., 2018; Yang et al., 2015), proteins related to not only glutamatergic but also dopaminergic and GABAergic synapses were also identified, including gephyrin (Figure 4B and Table S1).

Gephyrin is the major scaffold protein which interacts with the intracellular domains of $GABA_ARs$ and anchors them at the inhibitory postsynaptic membrane (Essrich et al., 1998; Kneussel et al., 1999; Mukherjee et al., 2011; Tretter et al., 2008). The cell adhesion molecule NL2 drives postsynaptic assembly at perisomatic inhibitory synapses via interaction with gephyrin and the membrane lipid-binding

protein collybistin (Poulopoulos et al., 2009). We speculated that endophilin A1 functions in the assembly of iPSD via interaction with the scaffold and/or intercellular adhesion proteins. To determine which inhibitory synaptic protein(s) interacts with endophilin A1, we performed coIP from HEK293T cells transiently expressing endophilin A1 and NL2, or gephyrin, and detected interaction of endophilin A1with gephyrin but not NL2 (Figure 4C and 4D). Moreover, coIP from mouse brain lysates corroborated interaction between endophilin A1 and gephyrin but not $GABA_AR$ α1 or γ2 (Figure 4E). Further, neither endophilin A2 nor A3 interacted with gephyrin (Figure 4F).

Notably, although the expression levels of gephyrin were not affected by ablation of *EEN1*, its distribution in the PSD fraction was decreased (Figure 3L). Consistently, immunofluorescence staining revealed a decrease in the clustering of gephyrin across the soma, the axon initial segment (AIS), and dendrites (Figure S4). The gephyrin clustering phenotype was rescued by expression of endophilin A1 but not endophilin A2 or A3 (Figure 4G,H), suggesting that their functions at the inhibitory postsynapses are not redundant. Conversely, overexpression of endophilin A1 caused an increase in the mean signal intensity and number of gephyrin puncta in the soma and dendrites (Figure 4I,J). Collectively, these data demonstrate that endophilin A1 interacts with the scaffold protein gephyrin and facilitates its clustering at inhibitory postsynapses.

At the submembraneous postsynaptic density, gephyrin self assembles via the N-terminal G and C-terminal E domains to provide scaffold for inhibitory postsynapses and anchors $GABA_ARs$ to the postsynaptic sites. Consistent with the effect of *EEN1* KO on the clustering of gephyrin (Figure 4G,H) and $GABA_AR$ γ2 (Figure 3A-D), immunofluorescence staining and confocal microscopy analysis showed that, depletion of endophilin A1 also caused a decrease in the localization of $GABA_AR$ γ2 to gephyrin puncta in *EEN1* KO neurons (Figure 5A-C). Moreover, overexpression of endophilin A1 also enhanced clustering of $GABA_AR$ γ2 in the soma and dendrites (Figure 5D,E). Together these data indicate that endophilin A1 promotes anchoring of $GABA_ARs$ to the iPSD.

To further understand the mechanism by which endophilin A1 regulates the assembly and function of inhibitory postsynapses, next we attempted domain mapping of the endophilin A1-gephyrin interaction. To this end, we generated a series of truncation and internal deletion mutants for endophilin A1 (Figure 5F). For those which did not express in mammalian cells, we determined their interaction with gephyrin by in vitro binding assays with recombinant proteins. None of the truncation or internal deletion mutants lost the ability to bind to gephyrin, and deletion of neither the BAR nor the SH3 domain weakened the binding (Figure 5G,H), suggesting that they are involved in the interaction with gephyrin. Indeed, the decreases in clustering of either gephyrin or $GABA_AR$ γ2 in *EEN1* KO neurons were not rescued by expression of endophilin A1 fragments (Figure 5I-L), indicating that all functional domains of endophilin A1 are required for the assembly of the GABAergic postsynaptic machinery.

Actin polymerization is required for stabilization of inhibitory postsynapses

Endophilin A1 functions in the morphogenesis and structural plasticity of dendritic spines by promoting actin polymerization underneath the plasma membrane (Yang et al., 2021; Yang et al., 2018; Yang et al., 2015). Of note, previous studies reported controversial results about the role of the actin and microtubule cytoskeleton in gephyrin clustering (Allison et al., 2000; Charrier et al., 2006; Kirsch and Betz, 1995). To further investigate the mechanism underlying endophilin A1-mediated assembly of inhibitory postsynapses, we asked whether actin polymerization contributes to the stabilization of iPSD and $GABA_AR$ clustering in dendrites. Consistent with previous studies (van Bommel et al., 2019), we observed large patches of F-actin labeled by LifeAct-mCherry in spines and small puncta in dendritic shafts that exhibited partial colocalization with or adjoined gephyrin in cultured hippocampal neurons by super-resolution microscopy (Figure S5A and Video S5). We then determined the impact of F-actin depolymerization on gephyrin-labeled iPSD and γ2-containing $GABA_ARs$ in cultured hippocampal neurons. One-hour or two-hour treatment of

mature neurons with nocodazole, a microtubule depolymerizing reagent, caused decreases in the number of both PSD95 and gephyrin puncta (Figure 6A-D), which was in good agreement with previous findings that microtubule dynamics regulates the spatial organization of both excitatory and inhibitory postsynaptic structures (Gu et al., 2008; Jaworski et al., 2009; Kirsch and Betz, 1995; Kirsch et al., 1991). Short-term or long-term incubation with latrunculin A, which disrupts actin polymerization, also caused decreases in the number of both ePSD and iPSD puncta (Figure 6A-D), indicating that actin polymerization also contributes to the stabilization of the iPSD. We then tested the effect of actin depolymerization on $GABA_AR$ clustering and found that, long-term but not short-term latrunculin A application caused a reduction in the number of $GABA_AR$ γ2 puncta in dendrites (Figure 6E-H), this finding supported the observation that the decrease in gephyrin cluster preceded the reduction in $GABA_AR$ γ2 receptor cluster following latrunculin A treatment (Figure 6I). In addition, colocalization analysis revealed less recruitment of γ2 to gephyrin puncta even after short-term drug application, without changes in γ2 clustering (Figure 6J,K). Together, these data demonstrate that actin polymerization is essential for the stabilization of iPSD and anchoring of $GABA_ARs$ to the postsynaptic sites.

Both the membrane-binding and p140Cap-binding capacities of endophilin A1 are indispensable for its function at the inhibitory postsynapses

At the excitatory synapse, the plasma membrane-associated endophilin A1 regulates the morphogenesis, maturation and structural plasticity of dendritic spines by promoting branched actin polymerization underneath the postsynaptic membrane via its interaction with the cytoskeleton regulator p140Cap (Yang et al., 2021; Yang et al., 2018; Yang et al., 2015). Having established the requirement for both endophilin A1 and the actin cytoskeleton in the assembly and stabilization of the inhibitory postsynaptic structure, we speculated that regulation of inhibitory postsynapse assembly by endophilin A1 necessitated its plasma membrane-binding and actin

polymerization-promoting activities. Silencing p140Cap expression in postsynaptic CA1 pyramidal cells by shRNA-mediated knockdown caused decreases in the clustering of gephyrin puncta in dendrites, which was restored by overexpression of p140Cap (Figure S5B,S5C), suggesting that p140Cap-mediated actin polymerization is required for the assembly of iPSD in postsynaptic neurons. However, compared with mere depletion of endophilin A1, p140Cap knockdown did not further attenuate the clustering of gephyrin in *EEN1* KO neurons (Figure S5D,S5E). Moreover, overexpression of p140Cap did not rescue the iPSD phenotype in *EEN1* KO neurons (Figure 7A,B), suggesting that p140Cap-enhanced actin polymerization promotes the organization of iPSD through endophilin A1-mediated pathway. Indeed, overexpression of neither the membrane-binding deficient (KKK-EEE) nor the p140Cap-binding deficient (Y343A) mutant of endophilin A1 (Yang et al., 2021) could rescue the iPSD defect (Figure 7A,B). Consistently, neither p140Cap nor the endophilin A1 loss-of-function mutants could rescue the $GABA_AR$ γ2 clustering phenotype in *EEN1* KO neurons (Figure 7C,D). Collectively, these data indicate that both plasma membrane association and actin polymerization-promoting activities are required for endophilin A1 to promote the assembly of the inhibitory postsynaptic machinery.

Next, we determined the mechanistic role of endophilin A1 in vivo by rescuing the epilepsy susceptibility caused by *EEN1* KO. Indeed, when AAVs expressing the Cre recombinase and endophilin A1 were co-injected into the hippocampal CA1 region of *EEN1*$^{fl/fl}$ mice, only the wild-type but not the membrane-binding or p140Cap-binding deficient mutant of endophilin A1 rescued the early onset and severity of PTZ-induced seizures (Figure 7E,F and Video S6). Consistently, electrophysiological recording in acute brain slices indicated that only wild-type endophilin A1 but not the mutants restored the amplitude of eIPSC and E/I balance in *EEN1* KO neurons (Figure 7G-K). All together, these data indicate that endophilin A1 contributes to the structure and function of inhibitory synapses by promoting the submembrane assembly of iPSD and synaptic localization of the $GABA_ARs$, thereby

maintaining the balance of excitatory and inhibitory activities in neural circuits (Figure 8).

Discussion

Although collybistin is implicated in plasma membrane recruitment and clustering of gephyrin and $GABA_AR$ α2 (Saiepour et al., 2010), studies of collybistin KO mice showed that the $GABA_AR$ α3 subunit promotes gephyrin-mediated formation of inhibitory synapses in the absence of collybistin (Wagner et al., 2021), raising the possibility that formation of a subset of GABAergic synapses requires gephyrin-interacting membrane-associated proteins other than collybistin. In the present study, we identify endophilin A1 as a novel binding partner for gephyrin and demonstrate that it promotes the assembly of inhibitory synapses and clustering of $GABA_ARs$ at the iPSD. Loss of endophilin A1 activity causes impairment of inhibitory synaptic transmission in neuronal circuits and increases susceptibility to seizures. In the central nervous system, inhibitory interneurons are highly diverse in morphologies, molecular profiles and physiological functions. Presynaptic terminals from different types of interneurons target distinct subcellular compartments in postsynaptic pyramidal neurons where $GABA_A$ receptors of specific subunit compositions are located. Parvalbumin-expressing (PV+) interneurons usually contact the soma and proximal dendrites, whereas somatostatin-expressing (SST+) interneurons mainly innervate the dendrites of pyramidal cells (Klausberger and Somogyi, 2008). Although different inhibitory synapses localized in different subcellular compartments of postsynaptic neurons have distinct properties and express a diversity of synaptic proteins, gephyrin remains a core postsynaptic component (Favuzzi et al., 2019). Our study revealed that endophilin A1 promotes the clustering of gephyrin in all subcellular compartments of pyramidal neurons, indicating that endophilin A1 functions in the organization of inhibitory postsynapses innervated by various presynaptic interneurons.

Among the endophilin A proteins, endophilin A1 is the most abundant in the

brain (Milosevic et al., 2011). Although they have redundant roles in physiological or pathological functions (Milosevic et al., 2011), endophilin A1, but not A2 or A3, promotes spine morphogenesis and excitatory postsynaptic organization (Yang et al., 2018; Yang et al., 2015; Milosevic et al., 2011). Here, we uncover a previously unanticipated role for endophilin A1 at GABAergic synapses. By deleting endophilin As in specific neuron subtypes, we found that endophilin A1 regulates GABAergic postsynaptic compartments. Endophilin A1, rather than A2 or A3, interacts with gephyrin and modulates the inhibitory postsynaptic machinery. Although endophilin A1 might function redundantly with other endophilin As in synaptic vesicle recycling at the presynaptic site, it participates in the organization or reorganization of postsynaptic structures through specific binding to postsynaptic proteins, a function that cannot be fully replaced by other endophilin As at both excitatory and inhibitory postsynapses.

The membrane lipid-binding protein collybistin interacts with the trans-synaptic cell adhesion molecule NL-2 to recruit gephyrin and $GABA_AR$ α2 to the postsynaptic membrane (Kalscheuer et al., 2009; Kins et al., 2000; Poulopoulos et al., 2009; Saiepour et al., 2010). Adamtsl3 secreted from presynapses binds to the transmembrane protein DCC (Deleted in Colorectal Cancer) and controls its synaptic localization, which is required for the maintenance of GABAergic synapses in the adult brain (Cramer et al., 2023). Anchoring of the α5 subunit of $GABA_AR$ to the actin cytoskeleton through radixin, an actin-binding protein, facilitates its clustering (Loebrich et al., 2006). These findings underscore the necessity for investigation of mechanism(s) regulating the plasma membrane-iPSD-actin cytoskeleton interaction. As membrane-binding and actin polymerization-promoting activities of endophilin A1 are both required for its function in enhancing iPSD formation and γ2–containing $GABA_AR$ clustering to iPSD, we propose that membrane-bound endophilin A1 promotes postsynaptic assembly by coordinating the plasma membrane tethering of the postsynaptic protein complex and its stabilization with the actin cytomatrix (Figure 8). In contrast, clustering of β2/3 subunit-containing $GABA_ARs$ is

independent of the actin or microtubule cytoskeleton in hippocampal neurons (Allison et al., 2000; Kasaragod et al., 2022). Given that synaptic and extrasynaptic $GABA_A$Rs are composed of distinct subunits (Kasaragod et al., 2022; Koh et al., 2023), these findings indicate that the actin cytoskeleton plays distinct roles in the clustering and possibly dynamic changes in the subunit composition and subcompartmental localization of different types of $GABA_A$Rs. Of note, the subcellular distribution of gephyrin, which has a tubulin-binding motif, is not affected by depolymerization of F-actin or microtubule (Allison et al., 2000). Overall, the discrepancy in data about the involvement of the actin cytoskeleton in inhibitory synapses may be due to differences in drug concentration, treatment time, receptor subtypes and neuronal cell types (Mody and Pearce, 2004; Sexton et al., 2021).

The number of synaptic $GABA_A$ receptors is subject to alterations not only during development and neuronal plasticity but also during pathological processes such as epilepsy (Nusser et al., 1998). Synaptic $GABA_A$ receptors are recruited directly from extrasynaptic pools following exocytosis, and their endocytosis occurs exclusively at extrasynaptic sites (Bogdanov et al., 2006). Therefore, lateral diffusion of $GABA_A$Rs between synaptic and extrasynaptic sites and their iPSD anchoring are very important for their synaptic distribution (Thomas et al., 2005). In good agreement with the finding that $GABA_A$Rs stabilization at synapses depends on gephyrin clustering (Jacob et al., 2005), we found that decreases in gephyrin clustering precedes the reduction in surface $GABA_A$Rs following F-actin depolymerization (Figure 6). As the core scaffold protein in iPSD, gephyrin is highly enriched at the inhibitory postsynaptic sites and drives the formation of iPSD sheets via phase separation (Bai et al., 2021). As binding of gephyrin by its partner proteins inhibits the iPSD condensate formation via autoinhibition of the multivalent interactions between its E domain and $GABA_A$Rs (Bai et al., 2021; Hoffmann and Milovanovic, 2021; Liu et al., 2020), it is conceivable that endophilin A1 binding not only tethers the scaffold protein to the plasma membrane, but also releases it from the autoinhibitory conformation to facilitate the phase separation of the gephyrin-receptor

complexes. Whether the activity of endophilin A1 is regulated by neuronal activity to participate in the structural and functional remodeling of iPSD awaits further investigation.

At the presynaptic site of excitatory synapses, endophilin A1 functions in synaptic vesicle recycling by recruiting the clathrin-uncoating factor synaptojanin (Milosevic et al., 2011; Schuske et al., 2003; Verstreken et al., 2003). At the excitatory postsynapse, plasma membrane-associated endophilin A1 facilitates the morphogenesis, stabilization, maturation and plasticity of dendritic spines by promoting actin polymerization via its interaction with p140Cap (Yang et al., 2021; Yang et al., 2018; Yang et al., 2015). In this study, we demonstrate that endophilin A1 functions upstream of p140Cap in not only excitatory but also inhibitory postsynapses of excitatory neurons. Intriguingly, recent studies reported that p140Cap is present in the inhibitory presynaptic compartment and regulates GABAergic synaptogenesis and neurotransmission (Russo et al., 2019), raising the possibility that endophilin A1 and p140Cap also coordinate to regulate the organization and activity of GABAergic synapses at the inhibitory presynaptic site. Remodeling of inhibitory synapses and dendritic spines are spatially clustered by sensory inputs in the central nervous system (Chen et al., 2012). Notably, the turnover of inhibitory synapses outpace that of excitatory synapses (Chen et al., 2012). Therefore, it is conceivable that deficits in inhibitory synapses are much more severe in *EEN1* KO mice, leading to perturbation of the E/I balance and increased epileptic vulnerability.

Materials and Methods

Ethics statement

All animal experiments were approved by and performed in accordance with the guidelines of the Animal Care and Use Committee of Institute of Genetics and Developmental Biology, Chinese Academy of Sciences (Approval code: AP2022008). All animals were housed in standard mouse cages at 22-24°C on a 12 h light/dark cycle with access to food and water freely.

Animals

Generation of *EEN1*$^{fl/fl}$ and *EEN1*$^{-/-}$ (KO first) mice on the C57BL/6J background were as previously described. Genotyping of mouse lines was performed by genomic PCR of tail prep DNA from offspring with the following primer pairs: loxPF/loxPR: 5'-CAAGGACTCCCAGAGACCTAGCATC-3' and 5'-GAGATGGCGCAACGCAATTAAT-3' (A PCR product of 375 base pairs in *EEN1* KO first mice but none in wild-type mice). zptF/zptR: 5'-gtaagcggctctagcgcatgttct-3' and 5'-GCAGGGGCATGTAGGTGGCTCAAC-3' (A PCR product of 466 base pairs in wild-type mice, none in *EEN1*$^{-/-}$ mice, and of 627 base pairs in *EEN1*$^{fl/fl}$ mice).

Constructs and viruses

pCMV-Tag2B-EEN1, pCMV-Tag2B-p140Cap, pCMV-Tag2B-EEN1 Y343A, pCMV-Tag2B-EEN1 KKK-EEE, pCMV-Tag2B-EEN1 (aa172-352), pGEX-4T-1-SH3 (aa295-352) and LifeAct-mCherry constructs were described previously (Yang et al., 2021; Yang et al., 2015). pAOV-CAMKIIα-mCherry-2A-3FLAG were purchased from OBiO Technology (Shanghai) Corp. Ltd., (Shanghai, China). pNICE-NL2(-) (Plasmid #15246) and pCR3-FLAG-gephyrin P1 (Plasmid #68816) were purchased from Addgene (Chih et al., 2006; Tyagarajan et al., 2013). The pCMV-Tag3B-GPN construct was generated by cloning gephyrin cDNA amplified from pCR3-FLAG-gephyrin into pCMV-Tag3B (Clontech Laboratories, Inc.). The pGEX-4T-1 EEN1 ΔBAR (Δaa6-242) and pGEX-4T-1 EEN1 ΔSH3 (Δaa1-352) constructs were generated by cloning fragments amplified from pCMV-Tag2B-EEN1 into pGEX-4T-1. All constructs were verified by DNA sequencing. Viral particles of adeno-associated virus (AAV) carrying mCherry, EGFP, the Cre recombinase, EEN1 WT or mutants were purchased from OBiO Technology (Shanghai) Corp. Ltd., (Shanghai, China).

Antibodies

The following antibodies were obtained from commercial sources: rabbit anti-endophilin A1 (159 002, Synaptic Systems GmbH, Germany), mouse anti-Gephyrin (147 111, Synaptic Systems), guinea pig anti-gephyrin (147 318, Synaptic Systems), mouse anti-neuroligin 2 (129 511, Synaptic Systems), mouse anti-GluA1 (MAB2263, Millipore), rabbit anti-$GABA_AR$ α1 (06-868, Millipore Sigma), rabbit anti-$GABA_AR$ γ2 (224 003, Synaptic Systems), mouse anti-SYP (D-4) (sc-17750, Santa Cruz), rabbit anti-FLAG (F3165, Sigma-Aldrich), rabbit and mouse anti-RFP which recognizes DsRed and mCherry (PM005 and M165-3, Medical & Biological Laboratories, Naka-ku Nagoya, Japan); mouse anti-α-tubulin (T9026, Sigma-Aldrich), mouse anti-PSD95 (610495, BD Biosciences, San Diego, CA) and mouse anti-GST (M071-3, MBL) for western blotting (WB) and rabbit anti-VGAT (131 004, Synaptic Systems), mouse anti-PSD95 (75-028, NeuroMab, Davis, CA), guinea pig anti-Ankyrin G (386 004, Synaptic Systems), guinea pig anti $GABA_AR$ γ2 (224 004, Synaptic Systems) for immunofluorescence staining; Rabbit anti-p140Cap was described previously (Yang et al., 2015). Alexa Fluor dye-conjugated secondary antibodies for immunofluorescence staining were from Molecular Probes (Invitrogen, Carlsbad, CA, USA).

Pentylenetetrazole (PTZ)-kindling and seizure behavior scoring

To evaluate seizure susceptibility, 8-10-week-old male C57BL/6N mice were intraperitoneally administered with PTZ (25 mg/kg; K0250, Sigma-Aldrich) or saline (control) for 8-12 days, and the resulting seizure behaviors were video-recorded for the next 30 min. Seizure susceptibility was measured by rating seizures on a scale of 0 to 7 as follows (Van Erum et al., 2019): no abnormal behavior (0), reduced motility and prostate position (1), facial jerking (Schulz et al.), neck ierks (Huo et al.), clonic seizure (sitting) (4), clonic, tonic-clonic seizure (lving on belly) (5), clonic, tonic-clonic seizure (lving on side) and wild jumping (6), tonic extension, possibly leading to respiratory arrest and death (7).

Stereotaxic injection

For virus injection, 9-10-week-old naive male and female mice were anesthetized and stereotactically injected with viral particles in the hippocampal CA1 region as described (Yang et al., 2018). Briefly, mice were weighed and anesthetized with isoflurane (2% 2,2,2-tribromoethanol, Sigma), and secured in a stereotaxic apparatus. The scalp of mouse was cut along the midline between the ears after sterilized with iodophors and 75% (vol/vol) alcohol. Holes for inserting needle were drilled in the bilateral skull. Viral particles carrying pAOV-CAMKIIa-MCS-mCherry-3FLAG or pAOV-CAMKIIa-mCherry-2A-Cre and pAAV-CaMKIIα-EGFP-2A-MCS-3FLAG or pAAV-CaMKIIα-EGFP-2A-MCS-3FLAG-EEN1 WT or mutants (1.2 μL, 2.0×10^{12} viral genomes/mL) (OBiO Technology Corp., Ltd) were injected bilaterally into the hippocampal CA1 regions using the following coordinates relative to bregma: 2.0 mm posterior, 1.8 mm lateral, and 1.4 mm ventral at a rate of 0.125 μL/min using a microinjection system (World Precision Instruments). The needle was kept in place for 2 min before withdrawal, and the skin was sutured with surgical line. The virus-injected mice were tested for behavior two weeks later.

Immunofluorescence staining of brain sections

Mice (P21 or P60) were anesthetized and immediately perfused, brains were dissected out, fixed overnight in 4% (vol/vol) paraformaldehyde, incubated overnight with 30% sucrose in phosphate-buffered saline (PBS), and then sliced into 30 μm-thick coronal sections using a cryotome (Model CM-1950; Leica Biosystems). For immunostaining of brain sections, floating 30 μm-thick slices were rinsed with PBS and permeabilized in 0.4% Triton X-100 in 0.01M PBS for 30 min. Cyrosections were blocked with 2% BSA in PBS containing 0.4% Triton X-100 for 2 h at room temperature (RT), then incubated with primary antibodies overnight at 4 °C. Secondary antibodies conjugated with Alexa Fluor 488 or 555 were used for detection. Sections were then incubated with DAPI (Roche, Grenzach-Wyhlen, Germany) for nuclear staining for 3 min at RT. Following rinsing, cyrosections were mounted on gelatin-coated slides and covered

with coverslip with mounting medium. Confocal images were collected using the Spectral Imaging Confocal Microscope Digital Eclipse A1Si (Nikon, Tokyo, Japan) with a 40× Plan Fluo (NA 1.30) oil objective (Yang et al., 2018).

Cell culture, transfection and drug treatment

Primary hippocampal neurons were cultured as previously described (Yang et al., 2021). Briefly, Hippocampi were rapidly dissected under sterile conditions, kept in cold DMEM (4°C) with high glucose. Tissue was then digested with 0.25% trypsin solution at 37°C for 18-20 min, triturated in DMEM supplemented with 10% F12 (11765054, Gibco) and 10% FBS (Gibco, Carlsbad, CA, USA). Then the tissue was mechanically dissociated into single cells by gentle pipetting up and down. Neurons were plated at a density of ~3.0-3.5× 10^5 cells/well in poly-D-lysine (P6407, Sigma-Aldrich) -coated 6-well plate and at a density of 2.5–3.0×10^4 cells/well in 24-well plate. Four hours later, media was changed to Neurobasal A (NB-A) growth medium supplemented with 2% B27 supplement (17504-044, Gibco), 1% GlutaMAX (35050-061, Gibco) and 33 mM glucose. Culture media were changed by half volume with Neurobasal maintenance media once a week. The cultures were maintained at 37°C with 5% CO_2. Experiments were performed at DIV 14-16 unless otherwise stated. For neuronal transfection, hippocampal neurons (DIV11) were transfected using Lipofectamine-LTX (15338100, Invitrogen, ThermoFisher Scientific). For 12 mm coverslips in individual wells of a 24 well plate, 0.5 μg of DNA was mixed with 0.5 μL PLUS reagent in 50 μL of NB-A and incubated for 5 min at RT, then gently mixed with 1 μL Lipofectamine LTX in 50 μL NB-A and incubated for 20 min at RT. The DNA-Lipofectamine LTX mixture was then added to the neurons in NB-A at 37°C in 5% CO_2 for 1 h. Neurons were then rinsed with NB-A and incubated in the original medium at 37°C in 5% CO_2 for 3-4 days.

For HEK293T cell culture, DMEM supplemented with 10% FBS were used. Cell transfections were performed using Lipofectamine-2000 (11668019, Invitrogen, ThermoFisher Scientific) according to the manufacturer's instructions. Cells were

harvested 24-48 h post transfection.

For inhibitor treatment, primary neurons cultured on coverslips were pre-incubated with Latrunculin A (1 μM, 76343-93-6, Sigma-Aldrich), Nocodazole (1 μM, 31430-18-9, Sigma-Aldrich) for 60 min or 120 min.

Immunofluorescence staining of cultured neurons

Hippocampal neurons were fixed in 4% paraformaldehyde/4% sucrose in PBS at RT for 15 min, then permeabilized in 0.4% Triton X-100 in PBS for 10 min. After blocking with 2% BSA in PBS containing 0.4% Triton X-100 for 30 min at RT, neurons were incubated with primary antibodies for 1 h at RT or overnight at 4°C, and appropriate secondary antibodies conjugated with Alexa Fluor 488, Alexa Fluor 555, or Alexa Fluor 647 were used for detection. The primary antibody was diluted in a PBS-2% BSA solution and incubated overnight at 4°C. After washing with PBS three times, samples were incubated with Alexa Fluor secondary antibodies (1:2000, Thermo Fisher) for 1 h at RT, and mounted without bubbles.

Biotinylation of cell surface proteins

Surface biotinylation experiments were performed as previously described (Guo et al., 2022). Briefly, Neurons were washed with ice cold extracellular solution (ECS) (in mM: 125 NaCl, 2 $CaCl_2$, 2.5 KCl, 5 HEPES, 33 glucose, pH, 8.0) and incubated for 30 min with 0.8 mg/ml NHS-SS-Biotin (21327, Thermo Fisher Scientific) in ECS buffer at 37°C. After incubation, cells were washed once with PBS and the unbound biotin was quenched via two 8 min incubations with quenching buffer (20 mM glycine in PBS). Lysis was performed by mechanical scraping in ice-cold lysis buffer (50 mM Tris-Cl pH 7.4, 150 mM NaCl, 1% TritonX-100, 0.1% SDS). After rotating for 30 min at 4°C, lysates were centrifuged for 10 min at 14,000× *g* at 4°C. Balanced Pierce Streptavidin Agarose beads (25 μL, 20353, Thermo Fisher Scientific) were added to the supernatant. The mixture of lysates and beads were rotated at 4°C overnight and then washed twice with ice-cold lysis buffer. Beads were incubated

with 2× SDS sample buffer for 10 min at 37°C and biotinylated proteins were analyzed by immunoblotting.

Protein expression and purification

GST-tagged EEN1 or gephyrin fragments was expressed in *E. coli* BL21 (DE3). Cells were grown at 37°C in LB (g/L: tryptone 10, yeast extract 5, NaCl 10) supplemented with ampicillin. Cells were induced at OD600 of ~0.6 with 0.4 mM isopropyl-D-1-thiogalactopyranoside (IPTG, A600168-0005, Bio Basic Inc) for 4 h at 30°C or 16 h at 16°C. Cell pellets were resuspended in PBS supplemented with 0.2% Triton X-100 and 0.1 mM PMSF. Proteins were purified with Glutathione Sepharose 4B (GE17-0756-01, Sigma-Aldrich, St. Louis, MO, USA) according to the manufacturer's instructions.

GST-pull down, co-immunoprecipitation (IP) and immunoisolation

For GST-pull down assays, GST-fused protein EEN1 and its fragments were expressed and purified from *E. coli*. Myc-tagged GPN constructs were expressed in HEK293 cells for 48 h and lysates were prepared in a buffer (in mM: Tris-HCl 50, pH 7.4, NaCl 150, 1% NP-40, EDTA 2) plus protease inhibitors cocktail. Cell lysates were centrifuged at 12,000× *g* for 15 min at 4°C and the supernatant was incubated with individual GST-fused proteins conjugated with Glutathione-Sepharose beads for overnight at 4°C. Beads were washed five times with lysis buffer and boiled in 2× SDS sample buffer. Bound proteins were analyzed by immunoblotting.

For co-IP from brain lysates, the whole brain from 8-10-week-old WT and KO mice were dissected and homogenized in the pre-chilled lysis buffer (in mM: Tris-HCl 20, pH 7.4, NaCl 150, 1% NP-40, EDTA 5) plus protease inhibitor cocktail, followed by incubation on ice for 15 min. The lysates were then centrifuged at 12,000× *g* for 15 min and the supernatant was collected and incubated with anti-EEN1 antibody (2 μg) or control IgG overnight at 4°C, followed by incubation with 20 μL Dynabeads

Protein A (ThermoFisher, 10007D for rabbit antibody) for 2 h at 4°C. After washing the beads with the same lysis buffer four times, the bound proteins were incubated 2× SDS sample buffer at 37°C for 10 min and subjected to SDS-PAGE and Western blot with indicated antibodies.

For co-IP of proteins in HEK293T cells, cells were lysed with lysis buffer (in mM: 0.5% NP-40, Tris-HCl 50, pH 7.4, NaCl 150, EDTA 5) supplemented with protease inhibitors. Lysates were then centrifuged at 16,000× *g* for 15 min at 4°C. Cell lysates were incubated with anti-Flag Affinity Gel (A2220, Sigma-Aldrich) overnight at 4°C on a roller mixer. Immunoprecipitates were washed four times in lysis buffer and boiled in 2× SDS sample buffer, then subjected to SDS-PAGE and immunoblotting.

For immunoisolation of membrane proteins, hippocampi were homogenized with lysis buffer (in mM: Tris-HCl 20, pH 7.4, HEPES 10, pH 7.4, NaCl 150, sucrose 250, EDTA 0.5, pH 8.0) supplemented with protease inhibitors and centrifuged at 800× *g* for 15 min. The supernatants were collected and subjected to high-speed centrifugation at 100,000× *g* for 1 h (TLS-55 rotor, OptimaTMMAX Ultracentrifuge; Beckman Coulter, USA). The supernatants (S100) and pellets (P100, the membrane fraction) resuspended in lysis buffer were subjected to immunoisolation with Dynabeads Protein A (100-4D, Invitrogen, Carlsbad, CA, USA) coupled with 2 μg of rabbit anti-EEN1 or rabbit anti-$GABA_AR$ α1 antibody. Bound proteins were eluted by incubation with 2× SDS loading buffer at 37°C for 10 min and subjected to SDS-PAGE and immunoblotting.

PSD fractionation of brain lysates

PSD fractions from mouse brain were prepared as previously described (Yang et al., 2015). In brief, hippocampi were homogenized on ice with 20 strokes of a Teflon-glass homogenizer in 1 mL of HEPES-buffered sucrose (0.32 M sucrose, 4 mM HEPES, pH 7.4) containing freshly added protease inhibitors, then centrifuged at 800× *g* at 4°C to remove the pelleted nuclear fraction (P1). Supernatant (S1) was

centrifuged at 10,000× *g* for 15 min to yield the crude synaptosomal pellet (P2) and the pellet was washed once in 1 mL HEPES-buffered sucrose. P2 was lysed by hypoosmotic shock in 900 μL ice-cold 4 mM HEPES, pH 7.4 plus protease inhibitors, homogenized by pipetting and rotating for 30 min at 4 °C. The lysate was centrifuged at 25,000× *g* for 20 min to yield supernatant (S3, crude synaptic vesicle fraction) and pellet (P3, lysed synaptosomal membrane fraction). To prepare the PSD fraction, P3 was resuspended in 900 μL of ice-cold 50 mM HEPES, pH 7.4, 2 mM EDTA, plus protease inhibitors and 0.5% Triton X-100, rotated for 15 min at 4 °C and centrifuged at 32,000× *g* for 20 min to obtain the PSD pellet. PSD pellets were resuspended in 50 μL ice-cold 50 mM HEPES, pH 7.4, 2 mM EDTA plus protease inhibitors. Proteins were subjected to SDS-PAGE and immunoblotting.

Protein identification with mass spectrometry and pathway analysis

For identification of EEN1-interacting proteins, mouse brain was homogenized with lysis buffer (in mM: Tris-HCl 20, pH 7.4, HEPES 10, pH 7.4, NaCl 150, EDTA 1, 1% NP-40) supplemented with protease inhibitors. Lysates were centrifuged at 12,000× *g* for 15 min. The supernatants were incubated with rabbit anti-EEN1 antibody overnight at 4°C. Beads were rinsed with lysis buffer for five times and bound proteins were resolved by SDS-PAGE. Proteins in the gels were reduced with 10 mM DTT at 37°C for 1 h, then alkylated with 25 mM iodoacetamide at RT for 1 h in the dark before digestion with trypsin (T1426, Sigma-Aldrich; enzyme-to-substrate ratio 1:50) in 25 mM ammonium bicarbonate at 37°C overnight. Tryptic peptides were extracted from gel by sonication with a buffer containing 5% trifluoroacetic acid and 50% acetonitrile. The liquid was dried by SpeedVac, and peptides were resolubilized in 0.1% formic acid and filtered with 0.45 μm centrifugal filters before analysis with a TripleTOF 5600 mass spectrometer (AB SCIEX, Canada) coupled to an Eksigent nanoLC. Proteins were identified by searching the MS/MS spectra against the *Mus musculus* SwissProt database using the ProteinPilot 4.2 software. Carbamidomethylation of cysteine was set as the fixed modification. Trypsin was

specified as the proteolytic enzyme with a maximum of 2 miss cleavages. Mass tolerance was set to 0.05 Da and the false discovery rates for both proteins and peptides were set at 1%. For enrichment pathway analysis: Only proteins with intensity to IgG ratio of > 1.5 were considered in the analysis. These genes were analyzed by Gene Ontology (GO) Enrichment Analysis (http://bioinfo.org/kobas).

Electrophysiology

To knockout *EEN1* in the brain, *EEN1*$^{fl/fl}$ mice were injected with high-titer AAV stock carrying pAOV-CaMKIIα-mCherry-2A-Cre (AAV-mCherry-2A-Cre) (1~5 × 10^{13} IU/ml) in the hippocampal CA1 region within 24 h after birth. Newborn mice were anesthetized on ice for 4-5 min and then mounted in a custom ceramic mold to align the head along the X and Y axes, with lambda set as (X, Y) = (0, 0). The zero point of the Z axis was the position at which the injecting needle penetrated the skin. Approximately 10 nL of the viral solution was injected at each of the seven sites (coordinates in mm, [X, Y, Z] = [1.2, 1.2, 1.4/1.0/0.6] and [1.5, 1.0, 1.7/1.3/0.9/0.5]) targeting the hippocampus in each cerebral hemisphere using a microsyringe (Sutter Instrument, Novato, CA, USA) and beveled glass injection pipette (Yang et al., 2018). For the rescue experiment, P0 *EEN1*$^{fl/fl}$ mice were injected with a mixture of two high-titer AAV stocks: AAV-EGFP and AAV-mCherry or AAV-mCherry-2A-Cre; AAV-mCherry-2A-Cre and AAV-EGFP-2A-FLAG-EEN1, AAV-EGFP-2A-FLAG-EEN1 Y343A or AAV-EGFP-2A-FLAG-EEN1 KKK-EEE. Approximately 20 nL of the viral solution was injected at each of the seven sites. The injected pups were returned to the home cage and used for recording 2 weeks later.

To prepare acute brain slices for electrophysiological analyses, mice were anesthetized with tribromoethanol (330-390 mg/kg) (T48402, Sigma-Aldrich, St. Louis, MO, USA) and decapitated. Whole brains were removed promptly and placed in ice-cold oxygenated (95% O_2/5% CO_2) low-Ca^{2+}/high-Mg^{2+} high-sucrose cutting solution (in mM: KCl 2.5, $NaHCO_3$ 25, NaH_2PO_4 1.25, glucose 10, sucrose 210, Na-Ascorbate 1.3, $CaCl_2$ 0.5, $MgSO_4$ 7). Coronal 300 μm slices were obtained using a

vibrating tissue slicer (Leica VT1200S; Leica Biosystems, Wetzlar, Deutschland). Slices were immediately transferred to standard artificial cerebrospinal fluid (ACSF) (in mM: NaCl 119, KCl 2.5, $MgSO_4$ 1.3, $CaCl_2$ 2.5, glucose 11, $NaHCO_3$ 26.2, NaH_2PO_4 1, pH 7.3-7.4) at 33°C and continuously bubbled with 95% O_2/5% CO_2. After 30 min of incubation, slices were transferred to a recording chamber with the same extracellular buffer at room temperature (RT, ~25°C).

For whole-cell patch clamp recordings, brain slices were continuously perfused with standard ACSF at RT under visual control with differential interference contrast illumination on an upright microscope (BX51WI, Olympus, Tokyo, Japan) with a 40× water-immersion objective and a digital camera. The mCherry- and/or EGFP-positive hippocampal CA1 pyramidal neurons were identified by an epifluorescence microscope (pE-300, CoolLED Ltd, Andover, UK). Whole-cell recordings were performed on an AAV-infected neuron and a neighboring uninfected neuron. Patch clamp data were obtained using a Multiclamp 700B amplifier (Molecular Devices, San Jose, CA, USA), and signals were low-pass filtered at 2 kHz and digitized at 10 kHz using an Axon Digidata 1550B analog-to-digital board (Molecular Devices, San Jose, CA, USA).

To analyze evoked excitatory postsynaptic currents (eEPSCs), evoked inhibitory postsynaptic currents (eIPSCs), and paired-pause ratio, cells were recorded with 3-7 MΩ borosilicate glass patch pipettes filled with the intracellular solution (in mM: $CsMeSO_3$ 135, HEPES 10, EGTA 1, QX-314 3.3, MgATP 4, NaGTP 0.3, and Na_2-phosphocreatine 8, pH 7.3) (Horn and Nicoll, 2018), following stimulation of Schaffer collaterals with a bipolar stimulation electrode placed in the stratum radiatum of the CA1 region. EPSCs were measured at a holding potential of -70 mV, and IPSCs were recorded at +10 mV. Paired-pulse ratios of EPSCs were measured at a holding potential of -70 mV by applying two electrical stimulations at a 50 ms interval and calculating the ratio of the peak amplitudes. Paired-pulse ratios of IPSCs were measured at a holding potential of +10 mV by applying two electrical stimulations at a 200 ms interval and calculating the ratio of the peak amplitudes. E/I

ratios were measured by applying the same stimulation current and then calculating the ratio of the absolute values of the peak amplitudes of EPSCs and IPSCs. The miniature EPSCs and IPSCs were measured in the ACSF bath solution containing 1 μM tetrodotoxin (TTX, MSS0002, BGB Analytik AG, BL, Switzerland) at -70 mV and +10 mV, respectively, in the voltage-clamp mode. Data were collected and analyzed using the pClamp 10.6 software (Molecular Devices, San Jose, CA, USA).

All electrophysiological recordings were carried out blindly and all n numbers in the data figures indicate the number of recorded neurons. All chemicals were purchased from Sigma-Aldrich except otherwise noted.

Confocal and three-dimensional structured illumination microscopy (3D-SIM) image acquisition and analysis

Confocal images were collected using the Spectral Imaging Confocal Microscope Digital Eclipse C1Si (Nikon, Tokyo, Japan) with a 100× Plan Apochromat VC (NA 1.40) oil objective (4× optical zoom). Images were z projections of images taken at 0.25-μm step intervals. The number of planes, typically 5-7, was chosen to cover the entire dendrite from top to bottom. Images were captured using a 1024×1024 pixels screen for neuronal cells. Laser power, digital gain, and offset settings were identical in each experiment. Images were processed with the NIH ImageJ software and exported into Adobe Photoshop. Only brightness and contrast were adjusted for the whole frame, and no part of a frame was enhanced or modified in any way. Control and experimental group neurons which were to be directly compared were imaged with the same acquisition parameters.

For 3D-SIM, secondary antibodies conjugated with Alexa Fluor 568 were used and images were captured as described by Niu et al (Niu et al., 2017) on the DeltaVision OMX V4 imaging system (Applied Precision Inc, USA) with a 100× 1.4 oil objective (Olympus UPlanSApo), solid state multimode lasers (488, 593 and 642 nm) and electron-multiplying charge-coupled device (CCD) cameras (Evolve 512× 512, Photometrics, USA). Serial Z-stack sectioning was done at 125 nm intervals. The

microscope is routinely calibrated with 100 nm fluorescent spheres to calculate both the lateral and axial limits of image resolution. SIM image stacks were reconstructed using softWoRx 5.0 (Applied Precision) with the following settings: pixel size 39.5 nm; channel-specific optical transfer functions; Wiener filter 0.001000; discard Negative Intensities background; drift correction with respect to first angle; custom K0 guess angles for camera positions. Pixel registration was corrected to be less than 1 pixel for all channels using 100 nm Tetraspeck beads. Three dimensional images were reconstructed from z stacks. For clarity of display, small linear changes of brightness and contrast were performed on three-dimensional reconstructions.

For quantitative analysis of immunofluorescent signals in neurons, maximal projection images were created with the ImageJ software (https://imagej.net.) from 6-7 serial optical sections. Background was subtracted by using the “subtract background” function and the background level was held identical for all cells within each experiment. To examine the number and fluorescence intensity of signal puncta in soma or dendrites, the EGFP- or DsRed-labeled soma or dendrites were outlined automatically by using the “Wand Tool” function. The region of interest (ROI) in cultured neurons was defined along a segment of the dendrite according to the fluorescence signal distinguished from the background. Average values of fluorescence intensities in ROI (the total fluorescent intensity divided by the total area of a dendritic segment) were calculated by Analyze > measure. Gephyrin clusters were thresholded and confirmed visually to select appropriate clusters following a minimal size cut-off by using the “Analyze Particles” plugin of the ImageJ software. For colocalization quantifications, NIS-Elements Software was used as follows: region of interest (ROI) of dendritic segments was manually chosen, and thresholded using the “Threshold” function to remove background signals. Pearson's correlation coefficient and Manders overlap coefficient were analyzed by using the “Analyze Control > colocalization” function.

Statistical analysis

For all biochemical, cell biological and electrophysiological recordings, at least three independent experiments were performed (independent cultures, transfections or different mice). Statistical analysis was performed in GraphPad Prism 9.0 (GraphPad Software, La Jolla, CA). Data sets were tested for normality and direct comparisons between two groups were made using two-tailed Student's t test (t test, for normally distributed data) as indicated. To evaluate statistical significance of three or more groups of samples, one-way analysis of variance with a Tukey test was used. The statistical significance was defined as * $p < 0.05$, ** $p < 0.01$, *** $p < 0.001$, respectively. All data are presented as mean ± S.E.M.

Acknowledgments

We thank Drs Shiva Tyagarajan (Addgene #68816) and Peter Scheiffele (Addgene # 15246) for constructs. This work was supported by funding from the National Natural Science Foundation of China (NSFC 32271005 and 32070785 to Y. Yang, 31921002, 32270730 and 91954126 to J-J. Liu) and the State Key Laboratory of Molecular Developmental Biology (2022-MDB-KF-13).

The authors declare no competing financial interests.

Author contributions: J-J. Liu and Y. Yang conceived the project. Y. Yang and J-J. Liu designed and supervised research. X. Chen, D. Pan and Y. Yang performed experiments and analyzed the data. Y. Yang and J-J. Liu wrote the manuscript with help from all other authors.

References

Allison, D.W., Chervin, A.S., Gelfand, V.I., and Craig, A.M. (2000). Postsynaptic scaffolds of excitatory and inhibitory synapses in hippocampal neurons: maintenance of core components independent of actin filaments and microtubules. The Journal of neuroscience : the official

840 journal of the Society for Neuroscience *20*, 4545-4554.

841 Bademosi, A.T., Decet, M., Kuenen, S., Calatayud, C., Swerts, J., Gallego, S.F., Schoovaerts,
842 N., Karamanou, S., Louros, N., Martin, E.*, et al.* (2023). EndophilinA-dependent coupling
843 between activity-induced calcium influx and synaptic autophagy is disrupted by a
844 Parkinson-risk mutation. Neuron.

845 Bai, G., Wang, Y., and Zhang, M. (2021). Gephyrin-mediated formation of inhibitory
846 postsynaptic density sheet via phase separation. Cell research *31*, 312-325.

847 Bogdanov, Y., Michels, G., Armstrong-Gold, C., Haydon, P.G., Lindstrom, J., Pangalos, M.,
848 and Moss, S.J. (2006). Synaptic GABAA receptors are directly recruited from their
849 extrasynaptic counterparts. The EMBO journal *25*, 4381-4389.

850 Canitano, R., and Pallagrosi, M. (2017). Autism Spectrum Disorders and Schizophrenia
851 Spectrum Disorders: Excitation/Inhibition Imbalance and Developmental Trajectories.
852 Frontiers in psychiatry *8*, 69.

853 Canitano, R., and Palumbi, R. (2021). Excitation/Inhibition Modulators in Autism Spectrum
854 Disorder: Current Clinical Research. Frontiers in neuroscience *15*, 753274.

855 Chang, D., Nalls, M.A., Hallgrímsdóttir, I.B., Hunkapiller, J., van der Brug, M., Cai, F., Kerchner,
856 G.A., Ayalon, G., Bingol, B., Sheng, M.*, et al.* (2017). A meta-analysis of genome-wide
857 association studies identifies 17 new Parkinson's disease risk loci. Nature genetics *49*,
858 1511-1516.

859 Charrier, C., Ehrensperger, M.V., Dahan, M., Lévi, S., and Triller, A. (2006). Cytoskeleton
860 regulation of glycine receptor number at synapses and diffusion in the plasma membrane. J
861 Neurosci *26*, 8502-8511.

862 Chen, J.L., Villa, K.L., Cha, J.W., So, P.T., Kubota, Y., and Nedivi, E. (2012). Clustered
863 dynamics of inhibitory synapses and dendritic spines in the adult neocortex. Neuron *74*,
864 361-373.
865 Chih, B., Gollan, L., and Scheiffele, P. (2006). Alternative splicing controls selective
866 trans-synaptic interactions of the neuroligin-neurexin complex. Neuron *51*, 171-178.
867 Corponi, F., Bonassi, S., Vieta, E., Albani, D., Frustaci, A., Ducci, G., Landi, S., Boccia, S.,
868 Serretti, A., and Fabbri, C. (2019). Genetic basis of psychopathological dimensions shared
869 between schizophrenia and bipolar disorder. Prog Neuropsychopharmacol Biol Psychiatry *89*,
870 23-29.
871 Cramer, T.M.L., Pinan-Lucarre, B., Cavaccini, A., Damilou, A., Tsai, Y.C., Bhat, M.A.,
872 Panzanelli, P., Rama, N., Mehlen, P., Benke, D.*, et al.* (2023). Adamtsl3 mediates DCC
873 signaling to selectively promote GABAergic synapse function. Cell reports *42*, 112947.
874 Dhir, A. (2012). Pentylenetetrazol (PTZ) kindling model of epilepsy. Current protocols in
875 neuroscience *Chapter 9*, Unit9.37.
876 Essrich, C., Lorez, M., Benson, J.A., Fritschy, J.M., and Luscher, B. (1998). Postsynaptic
877 clustering of major GABAA receptor subtypes requires the gamma 2 subunit and gephyrin.
878 Nature neuroscience *1*, 563-571.
879 Favuzzi, E., Deogracias, R., Marques-Smith, A., Maeso, P., Jezequel, J., Exposito-Alonso, D.,
880 Balia, M., Kroon, T., Hinojosa, A.J., E, F.M.*, et al.* (2019). Distinct molecular programs regulate
881 synapse specificity in cortical inhibitory circuits. Science *363*, 413-417.
882 Foss-Feig, J.H., Adkinson, B.D., Ji, J.L., Yang, G., Srihari, V.H., McPartland, J.C., Krystal, J.H.,
883 Murray, J.D., and Anticevic, A. (2017). Searching for Cross-Diagnostic Convergence: Neural

884 Mechanisms Governing Excitation and Inhibition Balance in Schizophrenia and Autism
885 Spectrum Disorders. Biol Psychiatry *81*, 848-861.
886 Fritschy, J.-M., Harvey, R.J., and Schwarz, G. (2008). Gephyrin: where do we stand, where do
887 we go? Trends in neurosciences *31*, 257-264.
888 Fritschy, J.M. (2008). Epilepsy, E/I Balance and GABA(A) Receptor Plasticity. Frontiers in
889 molecular neuroscience *1*, 5.
890 Gad, H., Ringstad, N., Low, P., Kjaerulff, O., Gustafsson, J., Wenk, M., Di Paolo, G., Nemoto,
891 Y., Crun, J., Ellisman, M.H.*, et al.* (2000). Fission and uncoating of synaptic clathrin-coated
892 vesicles are perturbed by disruption of interactions with the SH3 domain of endophilin. Neuron
893 *27*, 301-312.
894 George, S., Chiou, T.T., Kanamalla, K., and De Blas, A.L. (2021). Recruitment of Plasma
895 Membrane GABA-A Receptors by Submembranous Gephyrin/Collybistin Clusters. Cellular
896 and molecular neurobiology.
897 Germer, E.L., Imhoff, S., Vilariño-Güell, C., Kasten, M., Seibler, P., Brüggemann, N., Klein, C.,
898 and Trinh, J. (2019). The Role of Rare Coding Variants in Parkinson's Disease GWAS Loci.
899 Frontiers in neurology *10*, 1284.
900 Gu, J., Firestein, B.L., and Zheng, J.Q. (2008). Microtubules in dendritic spine development. J
901 Neurosci *28*, 12120-12124.
902 Guo, Z., Jiang, C.H., Tong, C., Yang, Y., Wang, Z., Lam, S.M., Wang, D., Li, R., Shui, G., Shi,
903 Y.S.*, et al.* (2022). Activity-dependent PI4P synthesis by PI4KIIIα regulates long-term synaptic
904 potentiation. Cell Rep *38*, 110452.
905 Han, W., Li, J., Pelkey, K.A., Pandey, S., Chen, X., Wang, Y.X., Wu, K., Ge, L., Li, T.,

906 Castellano, D.*, et al.* (2019). Shisa7 is a GABA(A) receptor auxiliary subunit controlling
907 benzodiazepine actions. Science *366*, 246-250.
908 Hoffmann, C., and Milovanovic, D. (2021). Gephyrin: a scaffold that builds a phase at the
909 inhibitory postsynapses. Cell research *31*, 245-246.
910 Horn, M.E., and Nicoll, R.A. (2018). Somatostatin and parvalbumin inhibitory synapses onto
911 hippocampal pyramidal neurons are regulated by distinct mechanisms. Proceedings of the
912 National Academy of Sciences *115*, 589-594.
913 Huo, J.Z., Cortez, M.A., and Snead, O.C., 3rd (2009). GABA receptor proteins within lipid rafts
914 in the AY-9944 model of atypical absence seizures. Epilepsia *50*, 776-788.
915 Jacob, T.C., Bogdanov, Y.D., Magnus, C., Saliba, R.S., Kittler, J.T., Haydon, P.G., and Moss,
916 S.J. (2005). Gephyrin regulates the cell surface dynamics of synaptic GABAA receptors. J
917 Neurosci *25*, 10469-10478.
918 Jaworski, J., Kapitein, L.C., Gouveia, S.M., Dortland, B.R., Wulf, P.S., Grigoriev, I., Camera, P.,
919 Spangler, S.A., Di Stefano, P., Demmers, J.*, et al.* (2009). Dynamic microtubules regulate
920 dendritic spine morphology and synaptic plasticity. Neuron *61*, 85-100.
921 Kalscheuer, V.M., Musante, L., Fang, C., Hoffmann, K., Fuchs, C., Carta, E., Deas, E.,
922 Venkateswarlu, K., Menzel, C., Ullmann, R.*, et al.* (2009). A balanced chromosomal
923 translocation disrupting ARHGEF9 is associated with epilepsy, anxiety, aggression, and
924 mental retardation. Human mutation *30*, 61-68.
925 Kasaragod, V.B., Mortensen, M., Hardwick, S.W., Wahid, A.A., Dorovykh, V., Chirgadze, D.Y.,
926 Smart, T.G., and Miller, P.S. (2022). Mechanisms of inhibition and activation of extrasynaptic
927 alphabeta GABA(A) receptors. Nature *602*, 529-533.

928 Kasaragod, V.B., and Schindelin, H. (2019). Structure of Heteropentameric GABAA Receptors
929 and Receptor-Anchoring Properties of Gephyrin. Frontiers in molecular neuroscience *12*, 191.
930 Kins, S., Betz, H., and Kirsch, J. (2000). Collybistin, a newly identified brain-specific GEF,
931 induces submembrane clustering of gephyrin. Nat Neurosci *3*, 22-29.
932 Kirsch, J., and Betz, H. (1995). The postsynaptic localization of the glycine
933 receptor-associated protein gephyrin is regulated by the cytoskeleton. The Journal of
934 neuroscience : the official journal of the Society for Neuroscience *15*, 4148-4156.
935 Kirsch, J., Langosch, D., Prior, P., Littauer, U.Z., Schmitt, B., and Betz, H. (1991). The 93-kDa
936 glycine receptor-associated protein binds to tubulin. J Biol Chem *266*, 22242-22245.
937 Klausberger, T., and Somogyi, P. (2008). Neuronal diversity and temporal dynamics: the unity
938 of hippocampal circuit operations. Science *321*, 53-57.
939 Kneussel, M., Brandstätter, J.H., Laube, B., Stahl, S., Müller, U., and Betz, H. (1999). Loss of
940 Postsynaptic GABAAReceptor Clustering in Gephyrin-Deficient Mice. J Neurosci *19*,
941 9289-9297.
942 Kneussel, M., Haverkamp, S., Fuhrmann, J.C., Wang, H., Wässle, H., Olsen, R.W., and Betz,
943 H. (2000). The gamma-aminobutyric acid type A receptor (GABAAR)-associated protein
944 GABARAP interacts with gephyrin but is not involved in receptor anchoring at the synapse.
945 Proc Natl Acad Sci U S A *97*, 8594-8599.
946 Koh, W., Kwak, H., Cheong, E., and Lee, C.J. (2023). GABA tone regulation and its cognitive
947 functions in the brain. Nature reviews Neuroscience *24*, 523-539.
948 Liu, Y.T., Tao, C.L., Zhang, X., Xia, W., Shi, D.Q., Qi, L., Xu, C., Sun, R., Li, X.W., Lau, P.M.*,*
949 *et al.* (2020). Mesophasic organization of GABAA receptors in hippocampal inhibitory

950 synapses. Nat Neurosci *23*, 1589-1596.

951 Loebrich, S., Bahring, R., Katsuno, T., Tsukita, S., and Kneussel, M. (2006). Activated radixin
952 is essential for GABAA receptor alpha5 subunit anchoring at the actin cytoskeleton. The
953 EMBO journal *25*, 987-999.

954 Miles, R., Tóth, K., Gulyás, A.I., Hájos, N., and Freund, T.F. (1996). Differences between
955 somatic and dendritic inhibition in the hippocampus. Neuron *16*, 815-823.

956 Milosevic, I., Giovedi, S., Lou, X., Raimondi, A., Collesi, C., Shen, H., Paradise, S., O'Toole, E.,
957 Ferguson, S., Cremona, O.*, et al.* (2011). Recruitment of endophilin to clathrin-coated pit
958 necks is required for efficient vesicle uncoating after fission. Neuron *72*, 587-601.

959 Mody, I., and Pearce, R.A. (2004). Diversity of inhibitory neurotransmission through GABA(A)
960 receptors. Trends in neurosciences *27*, 569-575.

961 Mukherjee, J., Kretschmannova, K., Gouzer, G., Maric, H.M., Ramsden, S., Tretter, V., Harvey,
962 K., Davies, P.A., Triller, A., Schindelin, H.*, et al.* (2011). The residence time of GABA(A)Rs at
963 inhibitory synapses is determined by direct binding of the receptor α1 subunit to gephyrin. J
964 Neurosci *31*, 14677-14687.

965 Murdoch, J.D., Rostosky, C.M., Gowrisankaran, S., Arora, A.S., Soukup, S.F., Vidal, R.,
966 Capece, V., Freytag, S., Fischer, A., Verstreken, P.*, et al.* (2016). Endophilin-A Deficiency
967 Induces the Foxo3a-Fbxo32 Network in the Brain and Causes Dysregulation of Autophagy and
968 the Ubiquitin-Proteasome System. Cell reports *17*, 1071-1086.

969 Niu, Y., Dai, Z., Liu, W., Zhang, C., Yang, Y., Guo, Z., Li, X., Xu, C., Huang, X., Wang, Y.*, et al.*
970 (2017). Ablation of SNX6 leads to defects in synaptic function of CA1 pyramidal neurons and
971 spatial memory. eLife *6*.

Nothdurfter, C., Tanasic, S., Di Benedetto, B., Uhr, M., Wagner, E.M., Gilling, K.E., Parsons, C.G., Rein, T., Holsboer, F., Rupprecht, R.*, et al.* (2013). Lipid raft integrity affects GABAA receptor, but not NMDA receptor modulation by psychopharmacological compounds. The international journal of neuropsychopharmacology *16*, 1361-1371.

Nusser, Z., Hajos, N., Somogyi, P., and Mody, I. (1998). Increased number of synaptic GABA(A) receptors underlies potentiation at hippocampal inhibitory synapses. Nature *395*, 172-177.

Parato, J., and Bartolini, F. (2021). The microtubule cytoskeleton at the synapse. Neuroscience letters *753*, 135850.

Poulopoulos, A., Aramuni, G., Meyer, G., Soykan, T., Hoon, M., Papadopoulos, T., Zhang, M., Paarmann, I., Fuchs, C., Harvey, K.*, et al.* (2009). Neuroligin 2 drives postsynaptic assembly at perisomatic inhibitory synapses through gephyrin and collybistin. Neuron *63*, 628-642.

Ren, Y., Xu, H.W., Davey, F., Taylor, M., Aiton, J., Coote, P., Fang, F., Yao, J., Chen, D., Chen, J.X.*, et al.* (2008). Endophilin I expression is increased in the brains of Alzheimer disease patients. The Journal of biological chemistry *283*, 5685-5691.

Ringstad, N., Gad, H., Low, P., Di Paolo, G., Brodin, L., Shupliakov, O., and De Camilli, P. (1999). Endophilin/SH3p4 is required for the transition from early to late stages in clathrin-mediated synaptic vesicle endocytosis. Neuron *24*, 143-154.

Ringstad, N., Nemoto, Y., and De Camilli, P. (1997). The SH3p4/Sh3p8/SH3p13 protein family: binding partners for synaptojanin and dynamin via a Grb2-like Src homology 3 domain. Proc Natl Acad Sci U S A *94*, 8569-8574.

Russo, I., Gavello, D., Menna, E., Vandael, D., Veglia, C., Morello, N., Corradini, I., Focchi, E.,

994 Alfieri, A., Angelini, C.*, et al.* (2019). p140Cap Regulates GABAergic Synaptogenesis and
995 Development of Hippocampal Inhibitory Circuits. Cerebral Cortex *29*, 91-105.
996 Saiepour, L., Fuchs, C., Patrizi, A., Sassoè-Pognetto, M., Harvey, R.J., and Harvey, K. (2010).
997 Complex role of collybistin and gephyrin in GABAA receptor clustering. J Biol Chem *285*,
998 29623-29631.
999 Sakimoto, Y., Oo, P.M., Goshima, M., Kanehisa, I., Tsukada, Y., and Mitsushima, D. (2021).
1000 Significance of GABAA Receptor for Cognitive Function and Hippocampal Pathology. Int J Mol
1001 Sci *22*.
1002 Schulz, A., Miehl, C., Berry, M.J., 2nd, and Gjorgjieva, J. (2021). The generation of cortical
1003 novelty responses through inhibitory plasticity. eLife *10*.
1004 Schuske, K.R., Richmond, J.E., Matthies, D.S., Davis, W.S., Runz, S., Rube, D.A., van der
1005 Bliek, A.M., and Jorgensen, E.M. (2003). Endophilin is required for synaptic vesicle
1006 endocytosis by localizing synaptojanin. Neuron *40*, 749-762.
1007 Scott, S., and Aricescu, A.R. (2019). A structural perspective on GABA(A) receptor
1008 pharmacology. Current opinion in structural biology *54*, 189-197.
1009 Sexton, C.A., Penzinger, R., Mortensen, M., Bright, D.P., and Smart, T.G. (2021). Structural
1010 determinants and regulation of spontaneous activity in GABAA receptors. Nature
1011 communications *12*, 5457.
1012 Soukup, S.F., Kuenen, S., Vanhauwaert, R., Manetsberger, J., Hernandez-Diaz, S., Swerts, J.,
1013 Schoovaerts, N., Vilain, S., Gounko, N.V., Vints, K.*, et al.* (2016). A LRRK2-Dependent
1014 EndophilinA Phosphoswitch Is Critical for Macroautophagy at Presynaptic Terminals. Neuron
1015 *92*, 829-844.

1016 Spruston, N. (2008). Pyramidal neurons: dendritic structure and synaptic integration. Nature
1017 reviews Neuroscience *9*, 206-221.
1018 Tao, C.L., Liu, Y.T., Sun, R., Zhang, B., Qi, L., Shivakoti, S., Tian, C.L., Zhang, P., Lau, P.M.,
1019 Zhou, Z.H.*, et al.* (2018). Differentiation and Characterization of Excitatory and Inhibitory
1020 Synapses by Cryo-electron Tomography and Correlative Microscopy. The Journal of
1021 neuroscience : the official journal of the Society for Neuroscience *38*, 1493-1510.
1022 Thomas, P., Mortensen, M., Hosie, A.M., and Smart, T.G. (2005). Dynamic mobility of
1023 functional GABAA receptors at inhibitory synapses. Nature neuroscience *8*, 889-897.
1024 Tretter, V., Jacob, T.C., Mukherjee, J., Fritschy, J.M., Pangalos, M.N., and Moss, S.J. (2008).
1025 The clustering of GABA(A) receptor subtypes at inhibitory synapses is facilitated via the direct
1026 binding of receptor alpha 2 subunits to gephyrin. The Journal of neuroscience : the official
1027 journal of the Society for Neuroscience *28*, 1356-1365.
1028 Tyagarajan, S.K., and Fritschy, J.M. (2014). Gephyrin: a master regulator of neuronal function?
1029 Nat Rev Neurosci *15*, 141-156.
1030 Tyagarajan, S.K., Ghosh, H., Yévenes, G.E., Imanishi, S.Y., Zeilhofer, H.U., Gerrits, B., and
1031 Fritschy, J.M. (2013). Extracellular signal-regulated kinase and glycogen synthase kinase 3β
1032 regulate gephyrin postsynaptic aggregation and GABAergic synaptic function in a
1033 calpain-dependent mechanism. The Journal of biological chemistry *288*, 9634-9647.
1034 van Bommel, B., Konietzny, A., Kobler, O., Bar, J., and Mikhaylova, M. (2019). F-actin patches
1035 associated with glutamatergic synapses control positioning of dendritic lysosomes. EMBO J *38*,
1036 e101183.
1037 Van Erum, J., Van Dam, D., and De Deyn, P.P. (2019). PTZ-induced seizures in mice require

1038 a revised Racine scale. Epilepsy & behavior : E&B *95*, 51-55.

1039 Verstreken, P., Koh, T.W., Schulze, K.L., Zhai, R.G., Hiesinger, P.R., Zhou, Y., Mehta, S.Q.,
1040 Cao, Y., Roos, J., and Bellen, H.J. (2003). Synaptojanin is recruited by endophilin to promote
1041 synaptic vesicle uncoating. Neuron *40*, 733-748.

1042 Wagner, S., Lee, C., Rojas, L., Specht, C.G., Rhee, J., Brose, N., and Papadopoulos, T.
1043 (2021). The α3 subunit of GABA(A) receptors promotes formation of inhibitory synapses in the
1044 absence of collybistin. J Biol Chem *296*, 100709.

1045 Watanabe, S., Mamer, L.E., Raychaudhuri, S., Luvsanjav, D., Eisen, J., Trimbuch, T.,
1046 Sohl-Kielczynski, B., Fenske, P., Milosevic, I., Rosenmund, C.*, et al.* (2018). Synaptojanin and
1047 Endophilin Mediate Neck Formation during Ultrafast Endocytosis. Neuron *98*, 1184-1197
1048 e1186.

1049 Yang, Y., Chen, J., Chen, X., Li, D., He, J., Wang, S., Zhao, S., Yang, X., Deng, S., Tong, C.*,*
1050 *et al.* (2021). Endophilin A1 drives acute structural plasticity of dendritic spines in response to
1051 Ca2+/calmodulin. The Journal of cell biology *220*.

1052 Yang, Y., Chen, J., Guo, Z., Deng, S., Du, X., Zhu, S., Ye, C., Shi, Y.S., and Liu, J.J. (2018).
1053 Endophilin A1 Promotes Actin Polymerization in Dendritic Spines Required for Synaptic
1054 Potentiation. Frontiers in molecular neuroscience *11*, 177.

1055 Yang, Y., Wei, M., Xiong, Y., Du, X., Zhu, S., Yang, L., Zhang, C., and Liu, J.J. (2015).
1056 Endophilin A1 regulates dendritic spine morphogenesis and stability through interaction with
1057 p140Cap. Cell research *25*, 496-516.

1058 Yu, Q., Wang, Y., Du, F., Yan, S., Hu, G., Origlia, N., Rutigliano, G., Sun, Q., Yu, H., Ainge, J.*,*
1059 *et al.* (2018a). Overexpression of endophilin A1 exacerbates synaptic alterations in a mouse

1060 model of Alzheimer's disease. Nature communications *9*, 2968.

1061 Yu, X., Xu, T., Ou, S., Yuan, J., Deng, J., Li, R., Yang, J., Liu, X., Li, Q., and Chen, Y. (2018b).

1062 Endophilin A1 mediates seizure activity via regulation of AMPARs in a PTZ-kindled epileptic

1063 mouse model. Experimental neurology *304*, 41-57.

1064

1065

Figure legends

Figure 1. Ablation of endophilin A1 in CA1 neurons disrupts the E/I balance and increases epilepsy susceptibility.

(A) Experimental protocol of PTZ kindling. Saline serves as negative control for PTZ.

(B) Representative images of convulsive behavior in each group.

(C) Seizures were monitored and scored after each injection. Nine 10-week-old mice were used in each condition. Seizure scores are shown as means ± S.E.M. Statistical test: * $p < 0.05$ and ** $p < 0.01$ compared with *EEN1*$^{+/+}$_PTZ.

(D) The representative mCherry-positive hippocampal CA1 neuron used for electrophysiological recording.

(E-F) Representative traces of evoked excitatory postsynaptic currents (eEPSC) and quantification of mean eEPSC amplitude (E), and paired-pulse recording (F) from 10 control (Ctrl, mCherry alone) and 10 *EEN1* KO (mCherry and Cre) pyramidal neurons.

(G-H) Representative traces of evoked inhibitory postsynaptic currents (eIPSCs) and quantification of mean eIPSC amplitude (G), and paired-pulse recording (H) from 9 control and 9 *EEN1* KO pyramidal neurons. Statistical test: * $p < 0.05$.

(I) Effect of *EEN1* KO on the E/I ratio from 9 control and 9 *EEN1* KO pyramidal neurons. Statistical test: * $p < 0.05$.

(J) Representative recordings of miniature excitatory postsynaptic currents (mEPSCs) traces (+10 mV) from control or *EEN1* KO CA1 pyramidal cells.

(K) Cumulative probability and quantification of mEPSC amplitude from 7 control and 7 *EEN1* KO pyramidal neurons.

(L) Cumulative probability and quantification of mEPSC frequency from 7 control and 7 *EEN1* KO pyramidal neurons.

(M) Representative recordings of miniature inhibitory postsynaptic currents (mIPSCs) traces (–70 mV) from control or *EEN1* KO CA1 pyramidal cells.

(N) Cumulative probability and quantification of mIPSC amplitude from 7 control and 7 *EEN1* KO pyramidal neurons.

(O) Cumulative probability and quantification of mIPSC frequency from 7 control and 7 *EEN1* KO pyramidal neurons. Statistical test: ns, non-significant. All data shown are means ± S.E.M.

Figure 2. *EEN1* KO causes defects in the formation and stabilization of inhibitory synapses.

(A-B) Immunofluorescence staining and confocal microscopy of gephyrin (GPN) in the hippocampal region of 3-week-old (P21) and 10-week-old (P60) *EEN1*$^{+/+}$ or *EEN1*$^{-/-}$ mouse brains. Scale bar, 50 μm.

(C) Quantification of the signal intensity of GPN in (A) and (B). n = 6 mice for each genotype.

(D-E) Same as (A-B) except that slices were immunostained for VGAT, (D) for P21, (E) for P60. Scale bar, 50 μm.

(F) Quantification of VGAT signal intensity in (D) and (E). n = 6 mice for each genotype.

(G-H) Same as (A-B) except that slices were immunostained for $GABA_AR$ γ2 (γ2). (G) for P21, (H) for P60. Scale bar, 50 μm.

(I) Quantification of γ2 signal intensity in (G) and (H). n = 6 mice for each genotype. Statistical test: * $p < 0.05$, ** $p < 0.01$, and *** $p < 0.001$; ns, non-significant. All data are means ± S.E.M. Abbreviations: CA1-3, cornus ammonis region 1-3; DG, dentate gyrus; DAPI staining of cell nuclei is shown in blue.

Figure 3. Endophilin A1 is distributed in the iPSD and regulates the assembly of the inhibitory postsynaptic machinery.

(A) Cultured *EEN1*$^{fl/fl}$ hippocampal neurons were transfected with construct expressing GFP or GFP-2A-Cre on DIV12, fixed and immunostained for surface GluA1 (sGluA1) or $GABA_AR$ γ2 (sγ2) on DIV16. Shown are representative confocal microscopy images. Lower panels are magnification of boxed regions in the upper panels. Scale bar, 10 μm in the upper panels and 5 μm in the lower panels.

(B) Quantification of the signal intensity (left) and cluster number (right) of GPN puncta in dendrites in (A). GFP: 56 segments of dendrites from 15 neurons; Cre: 70 segments of dendrites from 18 neurons.

(C-D) Cultured *EEN1*$^{fl/fl}$ hippocampal neurons were co-transfected with constructs for GFP or GFP-2A-Cre and Flag vector or Flag-endophilin A1 (Flag-EEN1) on DIV12, and immunostained for surface γ2 on DIV16. Shown are representative confocal images (C) and quantification of surface γ2 in dendrites (D). Scale bar, 5 μm. GFP: 60 segments of dendrites from 18 neurons; Cre: 59 segments of dendrites from 19 neurons; Cre + EEN1: 60 segments of dendrites from 18 neurons.

(E-F) *EEN1*$^{fl/fl}$ hippocampal neurons were infected with adeno-associated virus (AAV) carrying mCherry or mCherry-2A-Cre on DIV3 and surface biotinylated on DIV16. Total and surface proteins were detected by SDS-PAGE and immunoblotting. N = 3. LE: long exposure.

(G) Hippocampal neurons were transfected with construct expressing GFP to label neuronal morphology on DIV12, then immunostained with antibodies against EEN1 and GPN on DIV16. Shown are representative z stack maximum projection images captured by structured illumination microscopy (SIM). Lower panels are insets of boxed regions in the upper panel. Dendrites and spines are outlined in white. Scale bars, 2 μm in upper panels and 1 μm in magnified images.

(H) Same as (G) except that neurons were immunostained for EEN1 and surface γ2.

(I) Same as (G) except that neurons were immunostained for EEN1 and VGAT.

(J) Immunoisolation from the membrane fraction of mouse brain tissues with antibodies against $GABA_AR$ α1 (α1) or EEN1.

(K) Immunoisolation from *EEN1*$^{+/+}$ and *EEN1*$^{-/-}$ brain lysates with antibodies to $GABA_AR$ α1. Shown are representative immunoblot (left) and quantification of neuroligin 2 (NL2), GPN and $GABA_AR$ γ2 co-immunoisolated with α1 (right). N = 4 independent experiments.

(L) PSD fractions were isolated by differential centrifugation from mouse brain lysates and analyzed by immunoblotting with antibodies to EEN1 and synaptic proteins. S1, homogenates; PSD, postsynaptic density. SYP, synaptophysin. N = 4 independent experiments. Statistical test: * $p < 0.05$; ** $p < 0.01$; *** $p < 0.001$. ns: not significant. All data represent means ± S.E.M or scatterplots with means ± S.E.M.

Figure 4. Endophilin A1 interacts with gephyrin and promotes its clustering in postsynaptic neurons.

(A) Silver staining of proteins co-immunoprecipitated from *EEN1*$^{+/+}$ mouse brain lysates with antibodies to endophilin A1.

(B) Gene Ontology (GO) enrichment analysis of EEN1-interacting proteins identified by mass spectrometry.

(C-D) HEK293T cells co-transfected with constructs expressing Myc-tagged GPN or HA-tagged NL2 and Flag-tagged EEN1 for 48 h were lysed for Flag IP. Input and bound proteins were analyzed by immunoblotting with antibodies against Myc, HA and Flag.

(E) Co-IP from brain lysates with antibodies to EEN1.

(F) HEK293T cells overexpressing Flag-tagged endophilin As and Myc-tagged GPN were lysed for co-immunoprecipitation.

(G) *EEN1*$^{fl/fl}$ hippocampal neurons were co-transfected with constructs expressing GFP and Flag vector, or GFP-2A-Cre and Flag vector, Flag-EEN1, Flag-EEN2 or Flag-EEN3 on DIV12, fixed on DIV16 and immunostained for GPN, GFP and Flag. Shown are representative confocal microscopy images. Scale bar, 5 μm.

(**H**) Quantification of GPN signal intensity (left) and cluster number (right) in dendrites in (G). 52 dendrites from 14 neurons for GFP + vector; 58 dendrites from 15 neurons for Cre + vector; 59 dendrites from 16 neurons for Cre + EEN1; 44 dendrites from 14 neurons for Cre + EEN2; 45 dendrites from 11 neurons for Cre + EEN3.

(I) Hippocampal neurons were co-transfected with constructs expressing GFP and vector or Flag-EEN1 on DIV12, fixed and immunostained for GPN on DIV16. Shown are representative confocal microscopy images of GPN in the soma (left) and dendrites (right). Scale bars, 5 μm.

(J) Quantification of GPN signal intensity (left) and cluster number (right) in the soma and dendrites. 65 dendrites from 25 neurons for GFP + vector; 66 dendrites from 25 neurons for

GFP + EEN1. Statistical test: ** $p < 0.01$; *** $p < 0.001$. All data represent scatterplots with means ± S.E.M.

Figure 5. Both BAR and SH3 domains are required for endophilin A1-mediated organization of iPSD.

(A) *EEN1*$^{fl/fl}$ hippocampal neurons expressing GFP or Cre were immunostained for GPN, surface γ2 and GFP on DIV16. Shown are representative confocal microscopy images. Scale bars, 5 μm in left panels and 1 μm in magnified images.

(B-C) Quantification of the mean intensity of GPN (green) and surface γ2 (red) and their colocalization in (A). 18 neurons for GFP, 20 neurons for Cre.

(D) DIV12 hippocampal neurons were co-transfected with constructs expressing GFP and vector or Flag-EEN1, fixed on DIV16 and immunostained for surface γ2. Shown are representative confocal microscopy images of surface γ2 in the soma (left) and dendrites (right). Scale bars, 5 μm.

(E) Quantification of surface γ2 mean intensity (left) and cluster number (right) in the soma and dendrites. 68 dendrites from 20 neurons for GFP + vector, 61 dendrites from 20 neurons for GFP + EEN1.

(F) Schematic representation of EEN1 domain structure and diagrams of EEN1 fragments used for interaction mapping.

(G) GST-tagged EEN1 fragments conjugated to Glutathione-Sepharose beads were incubated with lysates of HEK293T cells overexpressing Myc-tagged GPN. Input and bound proteins were analyzed by immunoblotting with antibodies against Myc. Bottom panel: Coomassie blue-stained SDS-PAGE gel showing GST fusion proteins. FL, full length.

(H) HEK293T cells co-transfected with constructs encoding Myc-tagged GPN and Flag-tagged EEN1 fragments were lysed for Flag IP. Input and bound proteins were analyzed by immunoblotting with antibodies against Myc and Flag.

(I) DIV12 *EEN1*$^{fl/fl}$ hippocampal neurons were co-transfected with constructs expressing GFP and Flag vector or GFP-2A-Cre, and Flag vector or Flag-EEN1 FL, Flag-EEN1 ΔSH3, Flag-EEN1 aa172-352, fixed and immunostained for GPN on DIV16. Shown are representative confocal microscopy images of GPN. Scale bar, 5 μm.

(J) Quantification of mean intensity (left) and cluster number (right) in dendrites are shown for GPN in (I). Scale bar, 5 μm. 60 dendrites from 14 neurons for GFP + vector; 62 dendrites from 15 neurons for Cre + vector; 60 dendrites from 13 neurons for Cre + FL; 50 dendrites from 12 neurons for Cre + ΔSH3; 42 dendrites from 10 neurons for Cre + aa172-352.

(K) Same as (I) except that neurons were immunostained for surface γ2. Scale bar, 5 μm.

(L) Quantification of mean intensity (left) and cluster number (right) in dendrites are shown for surface γ2 in (K). 59 dendrites from 16 neurons for GFP + vector; 58 dendrites from 14 neurons for Cre + vector; 60 dendrites from 14 neurons for Cre + FL; 45 dendrites from 12 neurons for Cre + ΔSH3; 42 dendrites from 10 neurons for Cre + aa172-352. Statistical test: *

$p < 0.05$; ** $p < 0.01$; *** $p < 0.001$. All data represent scatterplots with means ± S.E.M.

Figure 6. Actin polymerization is required for stabilization of inhibitory postsynapses.

(A-D) DIV12 cultured hippocampal neurons transiently expressing GFP were treated with DMSO (vehicle control), 1 μM Latrunculin A (LatA) or 1 μM Nocodazole (Noco) for 60 min (A) or 120 min (C) on DIV16, respectively. Changes in postsynaptic proteins GPN (red) and PSD95 (green) were detected by confocal microscopy. Quantitative data shown were the mean intensity (left) and cluster number (right) of GPN and PSD95 at 60 min (B) and 120 min (D). Ctrl: 49 dendrites from 13 neurons for 60 min; 49 dendrites from 12 neurons for 120 min; LatA: 45 dendrites from 11 neurons for 60 min; 48 dendrites from 15 neurons for 120 min; Noco: 49 dendrites from 15 neurons for 60 min; 51 dendrites from 12 neurons for 120 min. Scale bar, 5 μm.

(E-H) Same as (A-D) except that neurons were immunostained for GPN (red) and surface γ2 (green). Changes in GPN and surface γ2 at 60 min (E) or 120 min (G) were detected by confocal microscopy. Quantitative data shown were the mean intensity (left) and cluster number (right) of GPN and surface γ2 at 60 min (F) and 120 min (H). Ctrl: 51 dendrites from 15 neurons for 60 min; 37 dendrites from 12 neurons for 120 min; LatA: 51 dendrites from 15 neurons for 60 min; 45 dendrites from 15 neurons for 120 min; Noco: 49 dendrites from 15 neurons for 60 min; 36 dendrites from 11 neurons for 120 min. Scale bar, 5 μm.

(I) Levels of synaptic proteins normalized to control neurons following LatA or Noco treatment in (A,C,E,G).

(J-K) The colocalization between surface γ2 and GPN signals in dendrites in (E) and (G). Statistical test: * $p < 0.05$; ** $p < 0.01$; *** $p < 0.001$. All data are scatterplots with means ± S.E.M.

Figure 7. Both the membrane-binding and p140Cap-binding capacities of endophilin A1 are required for iPSD assembly and E/I balance.

(A) Cultured hippocampal neurons from *EEN1*$^{fl/fl}$ mice were co-transfected with construct expressing GFP and Flag vector or GFP-2A-Cre and Flag vector, Flag-EEN1 wild-type (WT), mutants (KKK-EEE or Y343A) or p140Cap, and analyzed on DIV16 by immunofluorescence staining for GPN (green) and GFP (red). Scale bar, 5 μm.

(B) Quantification of GPN mean intensity (left) and cluster number (right) in (A). 65 dendrites from 14 neurons for GFP vector; 67 dendrites from 13 neurons for Cre + vector; 48 dendrites from 13 neurons for Cre + WT; 50 dendrites from 15 neurons for Cre + KKK-EEE; 52 dendrites from 14 neurons for Cre + Y343A; 62 dendrites from 14 neurons for Cre + p140Cap.

(C) Same as (A) except that neurons were immunostained for surface γ2 on DIV16. Scale bar, 5 μm.

(D) Quantification of surface γ2 mean intensity (left) and number (right) in (C). 40 dendrites from 11 neurons for GFP + vector; 38 dendrites from 10 neurons for Cre + vector; 40 dendrites from 11 neurons for Cre + WT; 45 dendrites from 14 neurons for Cre + KKK-EEE; 35 dendrites from 11 neurons for Cre + Y343A.

(E) Experimental scheme for seizure scoring of *EEN1*$^{fl/fl}$ mice stereotactically co-injected with AAVs carrying mCherry and Cre, and EGFP and EEN1 or its mutants (KKK-EEE and Y343A) in the hippocampal CA1 region. Mice were intraperitoneally administered PTZ for 12 days after AAV injections, then seizures were scored.

(F) PTZ-induced seizures in mice injected with the indicated AAVs were scored for 30 min. Ctrl, 7 mice; Cre, 7 mice; Cre + WT, 7 mice; Cre + KKK-EEE, 6 mice; Cre + Y343A, 7 mice.

(G-K) AAVs expressing Cre (AAV-mCherry-2A-Cre) and GFP (AAV-EGFP) or Cre and EEN1 WT or mutant (AAV-EGFP-2A-EEN1, AAV-EGFP-2A-EEN1 KKK-EEE, AAV-EGFP-2A-EEN1 Y343A) were stereotaxically injected into the CA1 regions of *EEN1*$^{fl/fl}$ mouse brain at P0. Acute hippocampal slices were prepared on P14-P21 for dual recording of evoked excitatory postsynaptic currents (eEPSC) and inhibitory postsynaptic currents (eIPSC). Shown are representative traces and pairwise comparisons of noninfected (Ctrl) and infected neurons in the same slice. Scale bar = 50/50, 50/50, 50/50, 50/50, 40/20 (pA/ms) in (G); Scale bar = 100/100, 100/400, 100/100, 100/200, 300/100 (pA/ms) in (H); Scale bar = 50/50, 50/50, 50/50, 50/50, 50/50 (pA/ms) in (I); Scale bar = 100/100, 200/100, 100/100, 100/200, 100/200 (pA/ms) in (J). Statistical test: * $p < 0.05$; ** $p < 0.01$; *** $p < 0.001$; red color is for Cre *vs* Ctrl, green color is for Cre + WT *vs* Cre; ns, not significant; All data are means ± S.E.M or scatterplots with means ± S.E.M.

Figure 8. Model for the role of endophilin A1 at the inhibitory postsynapses and E/I balance.

(A) Endophilin A1 directly interacts with the inhibitory postsynaptic scaffold protein gephyrin to promote organization of iPSD and synaptic recruitment/stabilization of the $GABA_A$Rs via its plasma membrane association and actin polymerization-promoting activities. **(B)** Loss of endophilin A1 impairs inhibitory synaptic neurotransmission and disrupts the balance of excitatory/inhibitory activities in the neural circuits, leading to enhanced epileptic seizure susceptibility.

Figure S1. Loss of endophilin A1 *in vivo* does not affect fast mIPSCs (perisomatic events: < 2.8 ms) and slow mIPSCs (distal dendritic events: >2.8 ms). Related to Figure 1

(A) Quantification of somatic and dendritic amplitudes in Ctrl and *EEN1* KO neuron. n = 7 WT and 9 *EEN1* KO neurons. Data are mean ± S.E.M.

(B) Frequency of somatic and dendritic events from Ctrl and *EEN1* KO mice. WT: 7 neurons; *EEN1* KO: 9 neurons. Data are mean ± S.E.M.

Figure S2. Effects of *EEN1* knockout on excitatory and inhibitory synapses in the hippocampus. Related to Figure 2

(A-B) Immunofluorescence analysis of PSD95 clusters in the hippocampal region of 3-week-old (P21) (left) and 10-week-old (P60) (right) $EEN1^{+/+}$ and $EEN1^{-/-}$ mouse brains. Scale bar, 50 μm.

(C) Quantification of the mean intensity of PSD95 in the hippocampal region of 3-week-old (P21) and 10-week-old (P60) $EEN1^{+/+}$ and $EEN1^{-/-}$ mouse brains. n = 3 mice for each genotype.

(D) Immunofluorescent signals of GPN in distinct layers of mouse hippocampus. Scale bar, 50 μm.

(E) Quantification of gephyrin (GPN) mean intensity in distinct layers of hippocampus. n = 6 mice for each genotype. Abbreviations: CA1-3, cornus Ammonis region 1-3; DG, dentate gyrus; slm, stratum lacunosum-moleculare; so, stratum oriens; sp, stratum pyramidale; sr, stratum radiatum. DAPI staining of cell nuclei is shown in blue. Statistical test: * $p < 0.05$; ** $p < 0.01$; *** $p < 0.001$; ns, non-significant. Data represent mean ± S.E.M.

Figure S3. Expression of $GABA_AR$ α1 in cultured hippocampal neurons. Related to Figure 3

Cultured hippocampal neurons were fixed on DIV16 and immunostained for surface $GABA_AR$ α1. Shown are representative confocal microscopy images. Scale bar, 10 μm.

Figure S4. Effect of *EEN1* knockout on gephyrin clustering in cultured hippocampal neurons. Related to Figure 4

(A-C) $EEN1^{fl/fl}$ hippocampal neurons were transfected with construct expressing mCherry or mCherry-2A-Cre on DIV12 and immunostained for GPN and mCherry on DIV16. Shown are representative confocal microscopy images for GPN in the soma, axon initial segment (AIS) and dendrites 30 μm, 60 μm, 90 μm or120 μm from the soma, respectively. Scale bars, 5 μm.

(D) Quantification of GPN mean intensity normalized to the mCherry group in the soma (A), AIS (B) and dendrites at various distances from the soma (C). Number: 20 (mCherry), 20 (Cre) for soma; 25 (mCherry), 25 (Cre) for AIS; 94 (mCherry), 76 (Cre) for dendrites 30 μm; 80 (mCherry), 51 (Cre) for dendrites 60 μm; 72 (mCherry), 61 (Cre) for dendrites 90 μm; 57 (mCherry), 41 (Cre) for dendrites 120 μm. Ankyrin-G: Axon initial segment (AIS) labeling marker. Statistical test: * $p < 0.05$, ** $p < 0.01$, *** $p < 0.001$. All data represent means ± S.E.M for each group.

Figure S5. p140Cap promotes gephyrin clustering via endophilin A1-mediated pathway. Related to Figure 6 and 7

(A) Cultured hippocampal neurons transiently expressing GFP and LifeAct-mCherry were immunostained for GPN, GFP and mCherry on DIV16. Shown are representative z stack maximum projection images captured by structured illumination microscopy (SIM). Right panels are insets of boxed regions in the left panel. Scale bars, 2 μm in left panels and 1 μm in magnified images.

(B) Cultured hippocampal neurons were co-transfected with Ctrl shRNA and vector or p140Cap shRNA and vector or RNAi-resistant Flag-tagged p140Cap on DIV 11, followed by immunostaining with antibodies to GPN, Flag (blue) and RFP on DIV 16. Scale bar, 5 μm.

(C) Quantification of GPN mean intensity and puncta number in (B). 82 dendrites from 18 neurons for shCtrl + vector; 92 dendrites from 20 neurons for shp140Cap + vector; 88 dendrites from 22 neurons for shp140Cap + p140Cap.

(D) *EEN1*$^{fl/fl}$ hippocampal neurons coexpressing GFP and Ctrl shRNA or p140Cap shRNA, or GFP-2A-Cre and Ctrl shRNA or p140Cap shRNA were immunostained for GPN on DIV16. Shown are representative confocal microscopy images. Scale bar, 5 μm.

(E) Quantification of GPN mean intensity and puncta number in (D). 59 dendrites from 14 neurons for GFP + shCtrl; 53 dendrites from 15 neurons for GFP + shp140Cap; 46 dendrites from 14 neurons for Cre + shCtrl; 63 dendrites from 17 neurons for Cre + shp140Cap. Statistical test: *** $p < 0.001$, ns, non-significant. All data shown are means ± S.E.M.

Table S1. Proteins identified by mass spec analysis of endophilin A1 co-immunoprecipitates and their abundance. Related to Figure 4

Video S1. PTZ kindling behaviors of *EEN1*$^{+/+}$ and *EEN1*$^{-/-}$ mice. Related to Figure 1

Video S2. The spatial relationship between EEN1 and GPN. **Related to Figure 3G**. 3D-SIM movie of an enlarged region of interest (ROI) from a hippocampal neuron dendrite shows the association of EEN1 (red) and GPN (green).

Video S3. The spatial relationship between endophilin A1 and surface GABA$_A$R γ2. **Related to Figure 3H**. 3D-SIM movie of an enlarged region of interest from a hippocampal neuron dendrite shows the association of EEN1 (red) and surface GABA$_A$R γ2 (green).

Video S4. The spatial relationship between endophilin A1 and VGAT. **Related to Figure 3I**. 3D-SIM movie of an enlarged region of interest from a hippocampal neuron dendrite shows the signals of EEN1 (red) and VGAT (green).

Video S5. The spatial relationship between gephyrin and LifeAct. Related to Figure 6 and Figure S5A. 3D-SIM movie of an enlarged region of interest from a hippocampal neuron dendrite shows the signals of LifeAct (red) and GPN (green).

Video S6. PTZ kindling behaviors of *EEN1*$^{fl/fl}$ mice injected with AAVs expressing Cre and EEN1 WT or mutants. Related to Figure 7

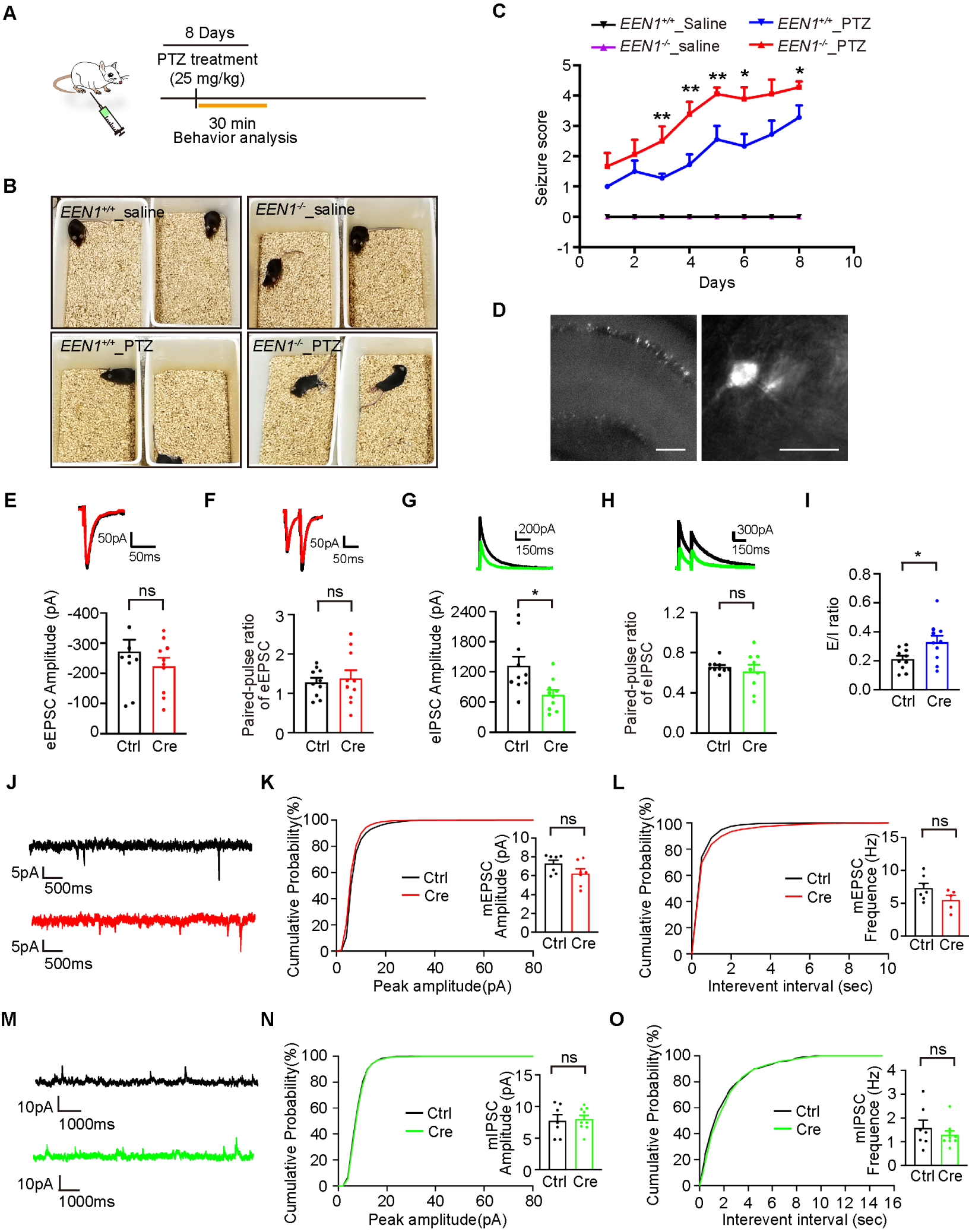
A
8 Days
PTZ treatment
(25 mg/kg)
30 min
Behavior analysis
B
EEN1+/+_saline
EEN1-/-_saline
EEN1+/+_PTZ
EEN1-/-_PTZ
C
EEN1+/+_Saline
EEN1+/+_PTZ
EEN1-/-_saline
EEN1-/-_PTZ
Seizure score
Days
D
E
50pA
50ms
eEPSC Amplitude (pA)
ns
Ctrl
Cre
F
50pA
50ms
Paired-pulse ratio of eEPSC
ns
G
200pA
150ms
eIPSC Amplitude (pA)
*
H
300pA
150ms
Paired-pulse ratio of eIPSC
ns
I
E/I ratio
*
J
5pA
500ms
K
Cumulative Probability(%)
Peak amplitude(pA)
Ctrl
Cre
mEPSC Amplitude (pA)
ns
L
Cumulative Probability(%)
Interevent interval (sec)
mEPSC Frequence (Hz)
ns
M
10pA
1000ms
N
Cumulative Probability(%)
Peak amplitude(pA)
mIPSC Amplitude (pA)
ns
O
Cumulative Probability(%)
Interevent interval (sec)
mIPSC Frequence (Hz)
ns

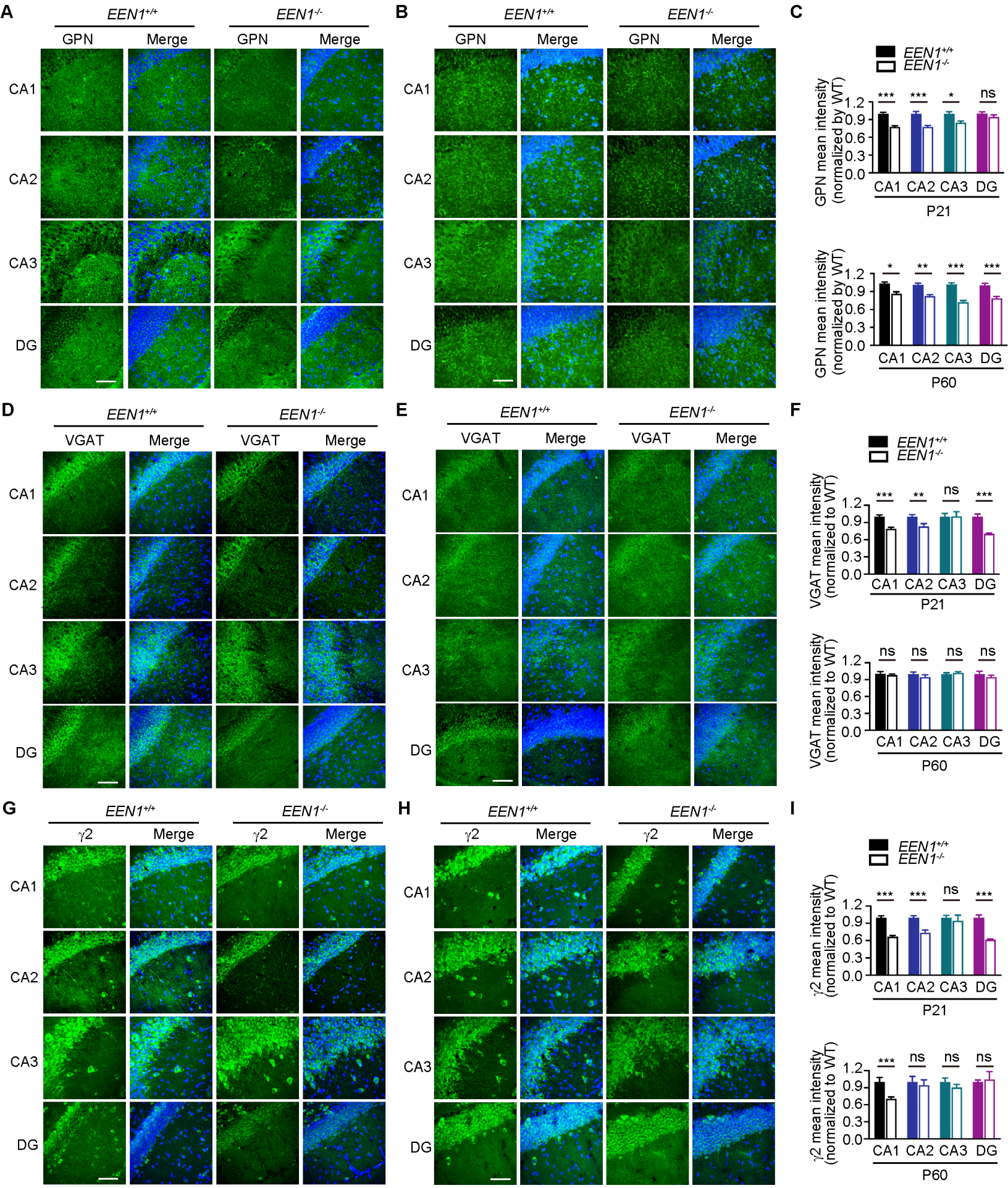
A
EEN1+/+
EEN1-/-
GPN
Merge
CA1
CA2
CA3
DG
B
C
GPN mean intensity (normalized by WT)
CA1 CA2 CA3 DG
P21
P60
D
VGAT
E
F
VGAT mean intensity (normalized to WT)
G
γ2
H
I
γ2 mean intensity (normalized to WT)

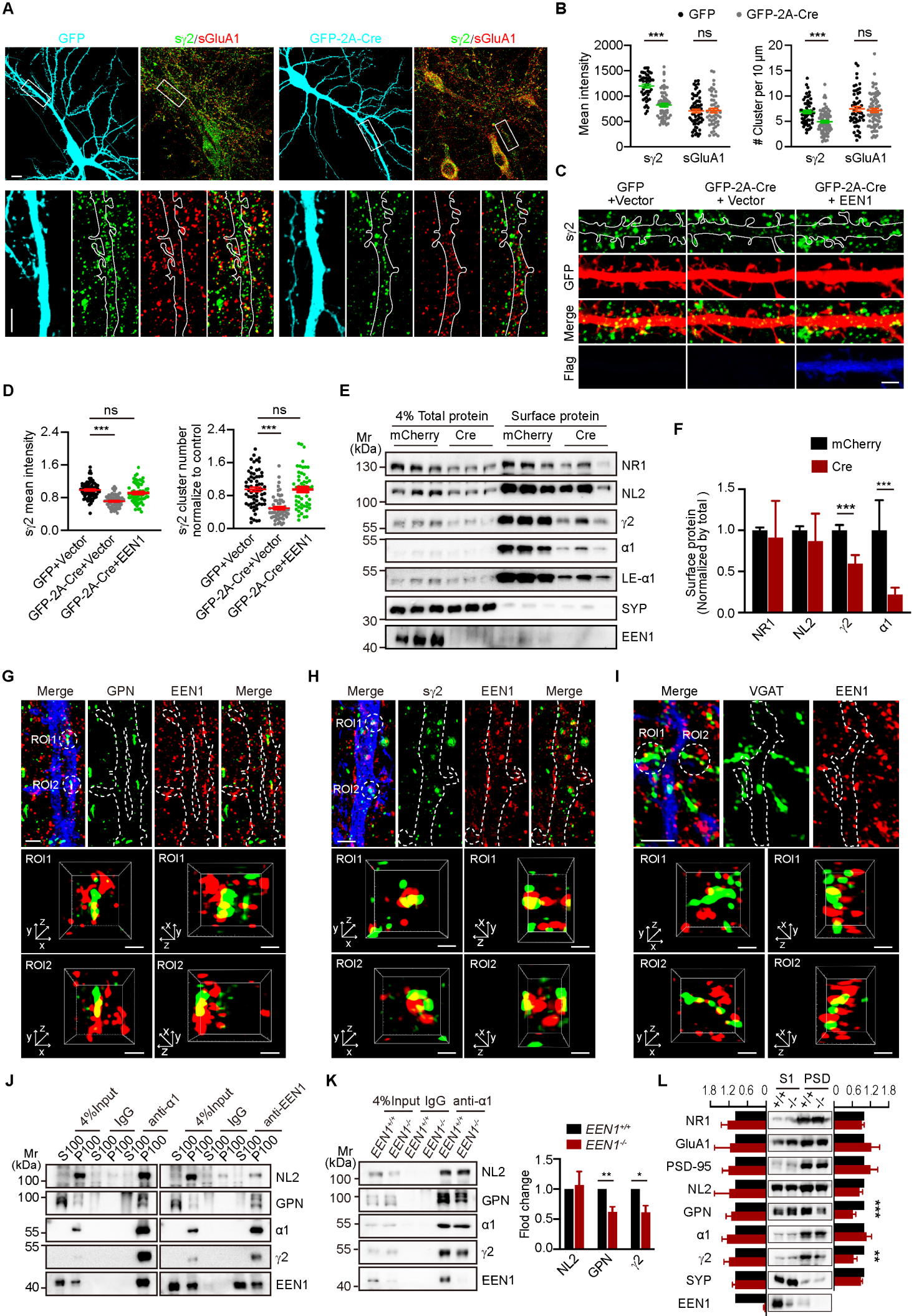
A
GFP
sγ2/sGluA1
GFP-2A-Cre
sγ2/sGluA1
B
GFP
GFP-2A-Cre
Mean intensity
Cluster per 10 μm
***
ns
sγ2
sGluA1
C
GFP +Vector
GFP-2A-Cre + Vector
GFP-2A-Cre + EEN1
sγ2
GFP
Merge
Flag
D
sγ2 mean intensity
sγ2 cluster number normalize to control
GFP+Vector
GFP-2A-Cre+Vector
GFP-2A-Cre+EEN1
E
4% Total protein
Surface protein
mCherry
Cre
Mr (kDa)
NR1
NL2
γ2
α1
LE-α1
SYP
EEN1
F
mCherry
Cre
Surface protein (Normalized by total)
NR1
NL2
γ2
α1
G
Merge
GPN
EEN1
ROI1
ROI2
H
sγ2
I
VGAT
J
4%Input
IgG
anti-α1
anti-EEN1
S100
P100
K
EEN1+/+
EEN1-/-
Flod change
L
S1
PSD
GluA1
PSD-95
GPN

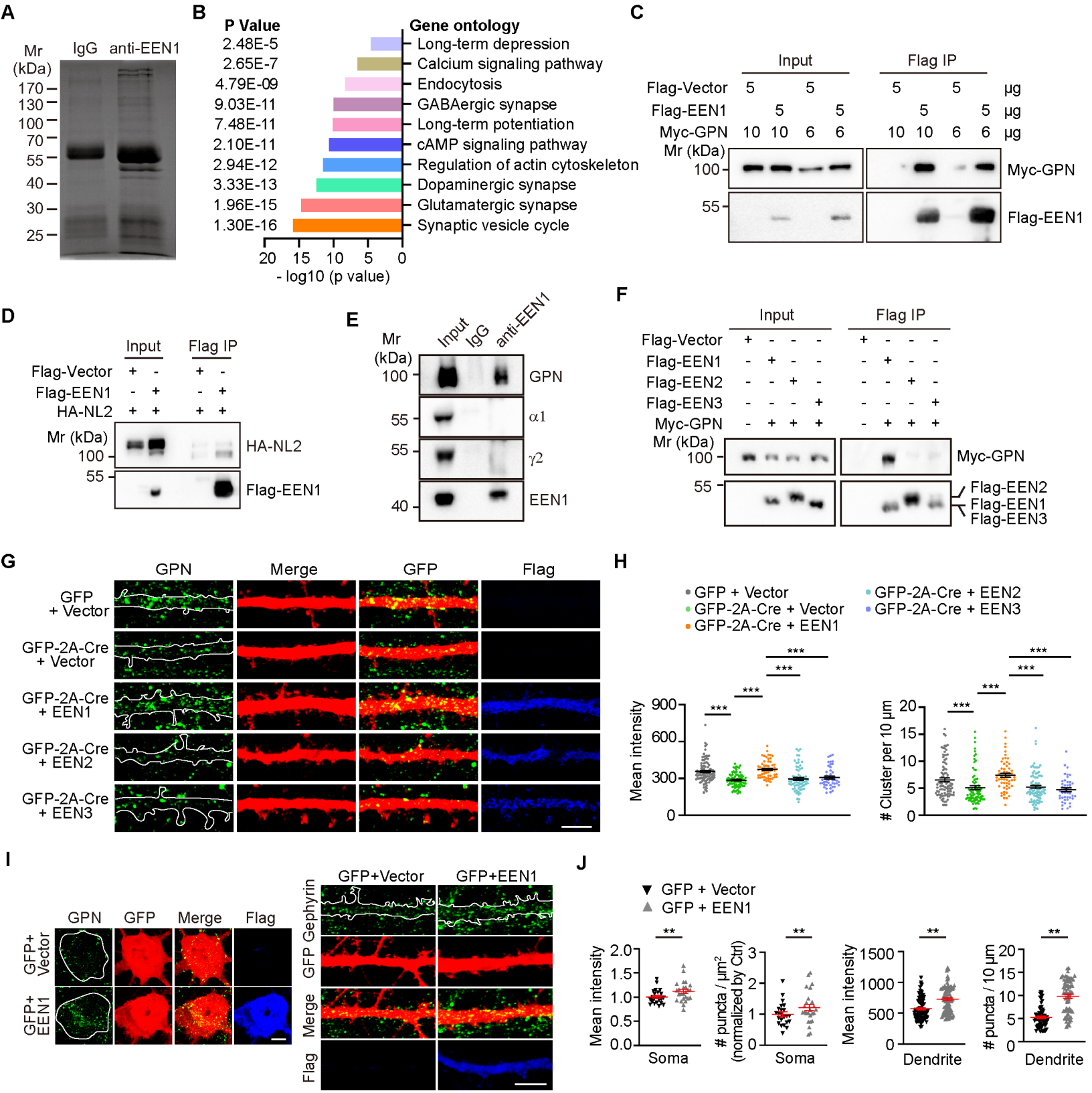
A
Mr (kDa)
IgG
anti-EEN1
170
130
100
70
55
40
30
25
B
P Value
Gene ontology
2.48E-5 Long-term depression
2.65E-7 Calcium signaling pathway
4.79E-09 Endocytosis
9.03E-11 GABAergic synapse
7.48E-11 Long-term potentiation
2.10E-11 cAMP signaling pathway
2.94E-12 Regulation of actin cytoskeleton
3.33E-13 Dopaminergic synapse
1.96E-15 Glutamatergic synapse
1.30E-16 Synaptic vesicle cycle
20 15 10 5 0
- log10 (p value)
C
Input
Flag IP
Flag-Vector 5 5 5 5 μg
Flag-EEN1 5 5 5 5 μg
Myc-GPN 10 10 6 6 10 10 6 6 μg
Mr (kDa)
100
55
Myc-GPN
Flag-EEN1
D
Input
Flag IP
Flag-Vector + - + -
Flag-EEN1 - + - +
HA-NL2 + + + +
Mr (kDa)
100
55
HA-NL2
Flag-EEN1
E
Mr (kDa)
Input
IgG
anti-EEN1
100
55
55
40
GPN
α1
γ2
EEN1
F
Input
Flag IP
Flag-Vector + - - - + - - -
Flag-EEN1 - + - - - + - -
Flag-EEN2 - - + - - - + -
Flag-EEN3 - - - + - - - +
Myc-GPN - + + + - + + +
Mr (kDa)
100
55
Myc-GPN
Flag-EEN2
Flag-EEN1
Flag-EEN3
G
GPN
Merge
GFP
Flag
GFP + Vector
GFP-2A-Cre + Vector
GFP-2A-Cre + EEN1
GFP-2A-Cre + EEN2
GFP-2A-Cre + EEN3
H
GFP + Vector
GFP-2A-Cre + Vector
GFP-2A-Cre + EEN1
GFP-2A-Cre + EEN2
GFP-2A-Cre + EEN3
Mean intensity
900
600
300
0
Cluster per 10 μm
20
15
10
5
0
***
I
GPN
GFP
Merge
Flag
GFP+ Vector
GFP+ EEN1
GFP+Vector
GFP+EEN1
GFP Gephyrin
Merge
Flag
J
GFP + Vector
GFP + EEN1
Mean intensity
2.0
1.5
1.0
0.5
0.0
Soma
puncta / μm² (normalized by Ctrl)
3
2
1
0
Soma
Mean intensity
1500
1000
500
0
Dendrite
puncta / 10 μm
20
15
10
5
0
Dendrite
**

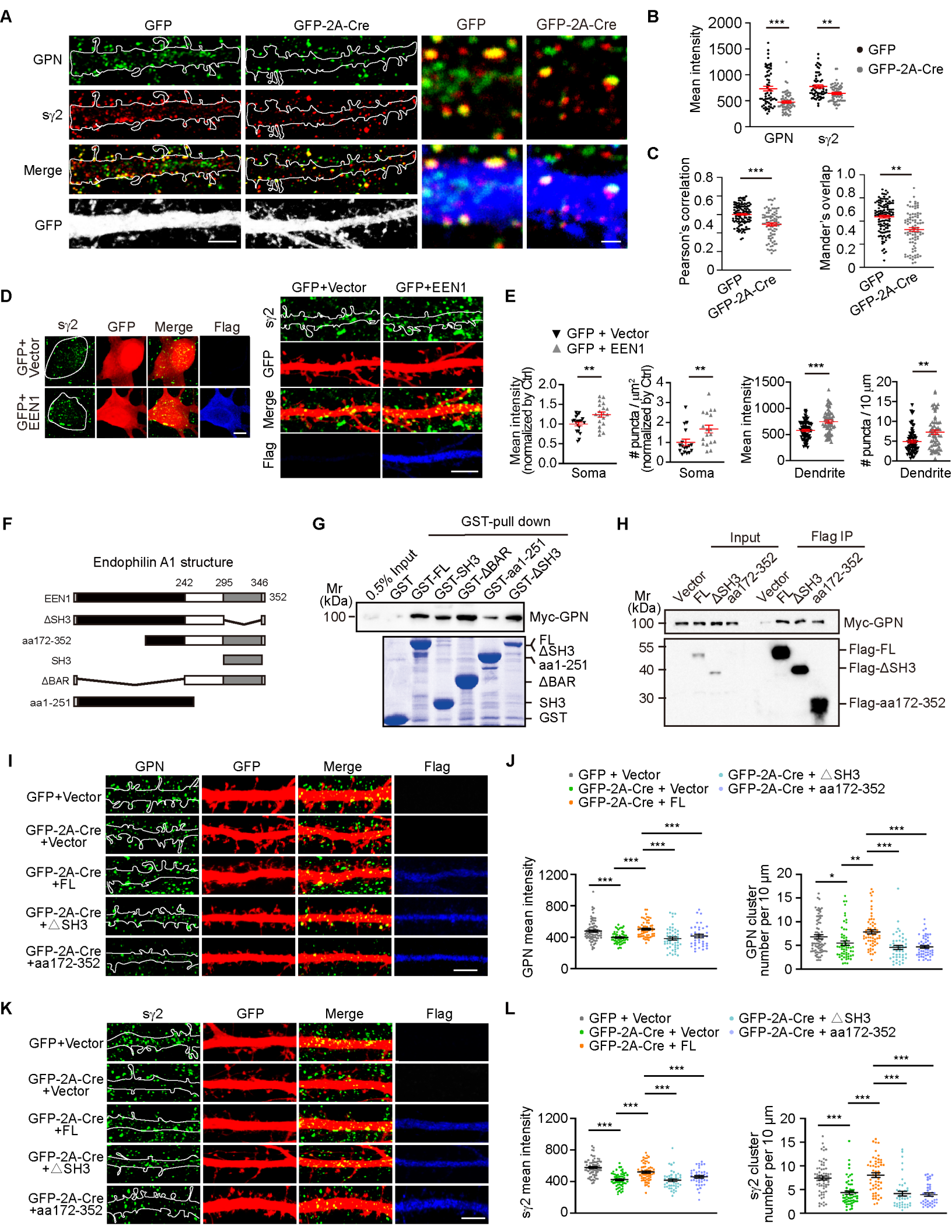
A
GFP
GFP-2A-Cre
GFP
GFP-2A-Cre
GPN
sγ2
Merge
GFP
B
Mean intensity
2000
1500
1000
500
0
***
**
GFP
GFP-2A-Cre
GPN
sγ2
C
Pearson's correlation
0.8
0.6
0.4
0.2
0
***
GFP
GFP-2A-Cre
Mander's overlap
1.0
0.8
0.6
0.4
0.2
0
**
GFP
GFP-2A-Cre
D
sγ2
GFP
Merge
Flag
GFP+ Vector
GFP+ EEN1
GFP+Vector
GFP+EEN1
sγ2
GFP
Merge
Flag
E
▼ GFP + Vector
▲ GFP + EEN1
Mean intensity (normalized by Ctrl)
2.0
1.5
1.0
0.5
0.0
**
Soma
puncta / μm² (normalized by Ctrl)
4
3
2
1
0
**
Soma
Mean intensity
1500
1000
500
0
***
Dendrite
puncta / 10 μm
20
15
10
5
0
**
Dendrite
F
Endophilin A1 structure
242
295
346
EEN1
352
ΔSH3
aa172-352
SH3
ΔBAR
aa1-251
G
GST-pull down
Mr (kDa)
0.5% Input
GST
GST-FL
GST-SH3
GST-ΔBAR
GST-aa1-251
GST-ΔSH3
100
Myc-GPN
FL
ΔSH3
aa1-251
ΔBAR
SH3
GST
H
Input
Flag IP
Mr (kDa)
Vector
FL
ΔSH3
aa172-352
Vector
FL
ΔSH3
aa172-352
100
Myc-GPN
55
40
30
Flag-FL
Flag-ΔSH3
Flag-aa172-352
I
GPN
GFP
Merge
Flag
GFP+Vector
GFP-2A-Cre +Vector
GFP-2A-Cre +FL
GFP-2A-Cre +△SH3
GFP-2A-Cre +aa172-352
J
GFP + Vector
GFP-2A-Cre + Vector
GFP-2A-Cre + FL
GFP-2A-Cre + △SH3
GFP-2A-Cre + aa172-352
GPN mean intensity
1200
800
400
0
***
***
***
***
***
GPN cluster number per 10 μm
20
15
10
5
0
*
**
***
***
***
K
sγ2
GFP
Merge
Flag
GFP+Vector
GFP-2A-Cre +Vector
GFP-2A-Cre +FL
GFP-2A-Cre +△SH3
GFP-2A-Cre +aa172-352
L
GFP + Vector
GFP-2A-Cre + Vector
GFP-2A-Cre + FL
GFP-2A-Cre + △SH3
GFP-2A-Cre + aa172-352
sγ2 mean intensity
1200
800
400
0
***
***
***
***
***
sγ2 cluster number per 10 μm
20
15
10
5
0
***
***
***
***
***

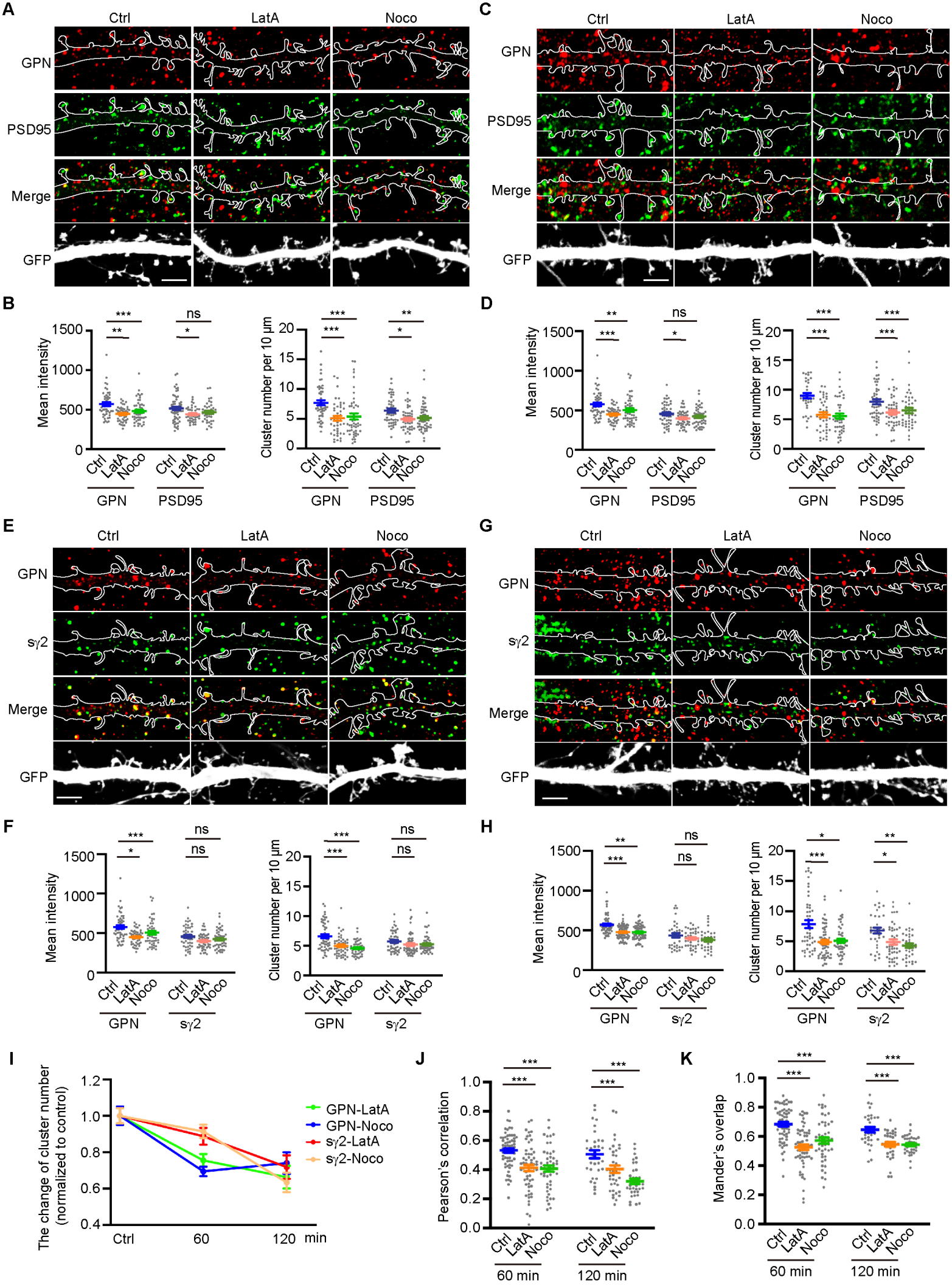
A
Ctrl
LatA
Noco
GPN
PSD95
Merge
GFP
B
Mean intensity
Cluster number per 10 μm
Ctrl
LatA
Noco
GPN
PSD95
C
D
E
sγ2
F
G
H
I
The change of cluster number (normalized to control)
GPN-LatA
GPN-Noco
sγ2-LatA
sγ2-Noco
min
J
Pearson's correlation
60 min
120 min
K
Mander's overlap

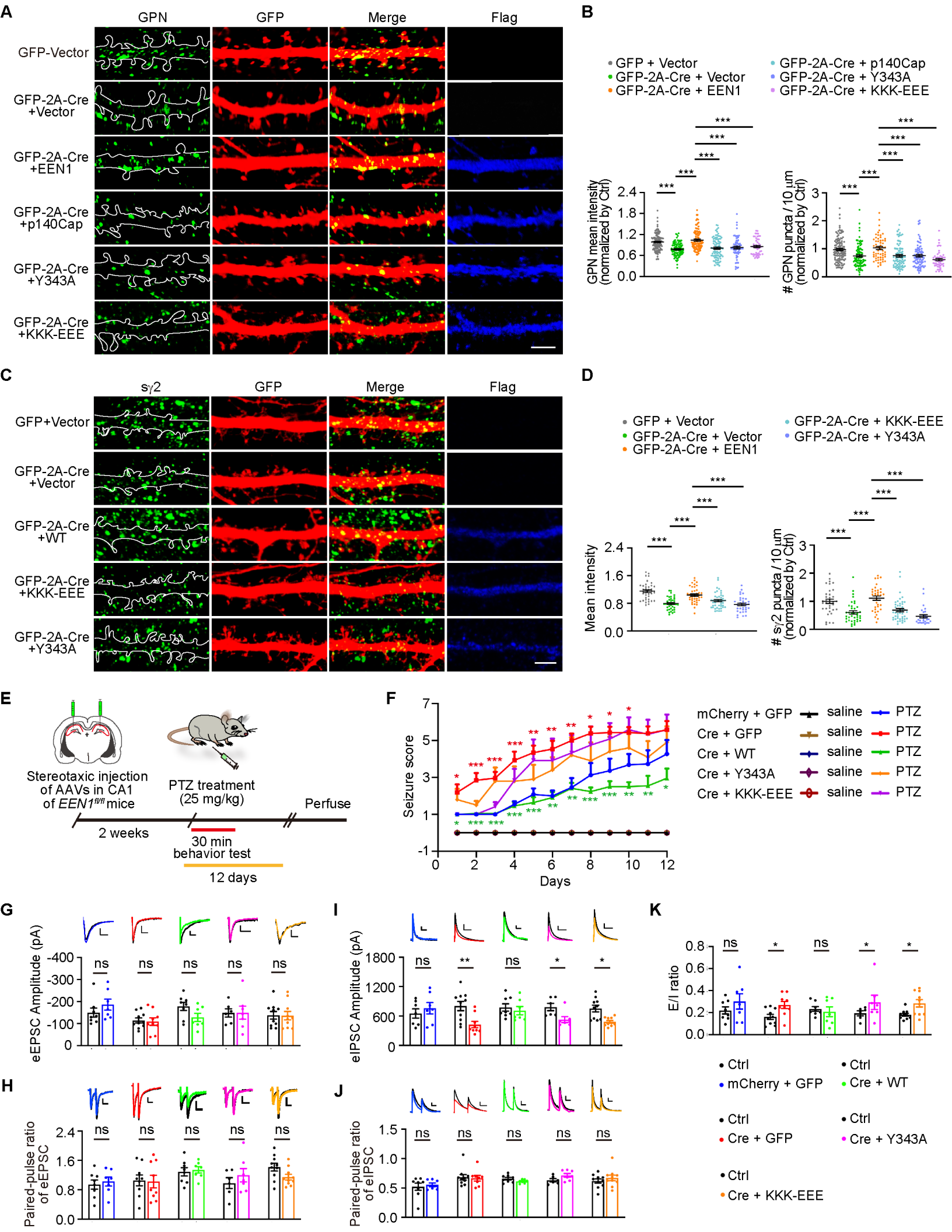
A
GPN
GFP
Merge
Flag
GFP-Vector
GFP-2A-Cre +Vector
GFP-2A-Cre +EEN1
GFP-2A-Cre +p140Cap
GFP-2A-Cre +Y343A
GFP-2A-Cre +KKK-EEE
B
GFP + Vector
GFP-2A-Cre + Vector
GFP-2A-Cre + EEN1
GFP-2A-Cre + p140Cap
GFP-2A-Cre + Y343A
GFP-2A-Cre + KKK-EEE
GPN mean intensity (normalized by Ctrl)
GPN puncta / 10 μm (normalized by Ctrl)
C
sγ2
GFP
Merge
Flag
GFP+Vector
GFP-2A-Cre +Vector
GFP-2A-Cre +WT
GFP-2A-Cre +KKK-EEE
GFP-2A-Cre +Y343A
D
GFP + Vector
GFP-2A-Cre + Vector
GFP-2A-Cre + EEN1
GFP-2A-Cre + KKK-EEE
GFP-2A-Cre + Y343A
Mean intensity
sγ2 puncta / 10 μm (normalized by Ctrl)
E
Stereotaxic injection of AAVs in CA1 of EEN1fl/fl mice
PTZ treatment (25 mg/kg)
Perfuse
2 weeks
30 min behavior test
12 days
F
Seizure score
Days
mCherry + GFP saline PTZ
Cre + GFP saline PTZ
Cre + WT saline PTZ
Cre + Y343A saline PTZ
Cre + KKK-EEE saline PTZ
G
eEPSC Amplitude (pA)
I
eIPSC Amplitude (pA)
K
E/I ratio
H
Paired-pulse ratio of eEPSC
J
Paired-pulse ratio of eIPSC
Ctrl
mCherry + GFP
Ctrl
Cre + WT
Ctrl
Cre + GFP
Ctrl
Cre + Y343A
Ctrl
Cre + KKK-EEE

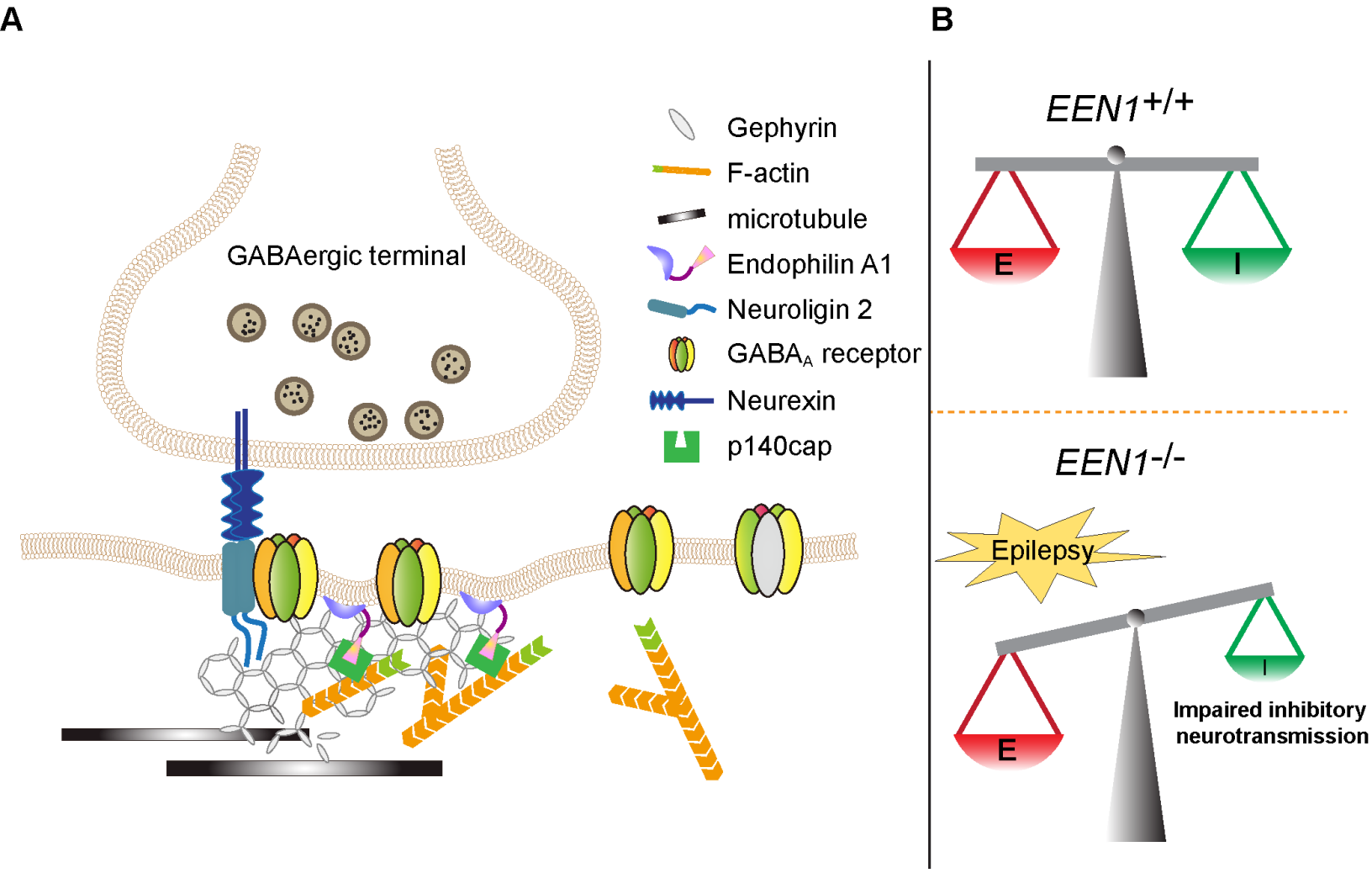
A
GABAergic terminal
Gephyrin
F-actin
microtubule
Endophilin A1
Neuroligin 2
GABA$_A$ receptor
Neurexin
p140cap
B
EEN1+/+
E
I
EEN1-/-
Epilepsy
E
I
Impaired inhibitory neurotransmission